



1 **Sulfur dioxide retrievals from TROPOMI onboard Sentinel-5**
2 **Precursor: Algorithm Theoretical Basis**

3 **N. Theys¹, I. De Smedt¹, H. Yu¹, T. Danckaert¹, J. van Gent¹, C. Hörmann², T.**
4 **Wagner², P. Hedelt³, H. Bauer³, F. Romahn³, M. Pedergnana³, D. Loyola³, M. Van**
5 **Roosendael¹**

6
7 [1]{Royal Belgian Institute for Space Aeronomy (BIRA-IASB), Brussels, Belgium}

8 [2]{Max Planck Institute for Chemistry (MPIC), Hahn-Meitner-Weg 1, 55128 Mainz,
9 Germany}

10 [3]{Institut für Methodik der Fernerkundung (IMF), Deutsches Zentrum für Luft und
11 Raumfahrt (DLR), Oberpfaffenhofen, Germany}

12
13 Correspondence to N. Theys (theys@aeronomie.be)

14
15 **ABSTRACT**

16 The TROPospheric Monitoring Instrument (TROPOMI) onboard the Copernicus Sentinel-5
17 Precursor (S-5P) platform will measure ultraviolet Earthshine radiances at high spectral and
18 improved spatial resolution (pixel size of 7x3.5 km² at nadir) compared to its predecessors
19 OMI and GOME-2. This paper presents the sulfur dioxide (SO₂) vertical column retrieval
20 algorithm implemented in the S-5P operational processor UPAS (Universal Processor for
21 UV/VIS Atmospheric Spectrometers), and comprehensively describes its various retrieval
22 steps. The spectral fitting is performed using the Differential Optical Absorption
23 Spectroscopy (DOAS) method including multiple fitting windows to cope with the large range
24 of atmospheric SO₂ columns encountered. It is followed by a slant column background
25 correction scheme to reduce possible biases or across-track dependent artifacts in the data.
26 The SO₂ vertical columns are obtained by applying Air Mass Factors (AMF) calculated for a
27 set of representative a-priori profiles and accounting for various parameters influencing the
28 retrieval sensitivity to SO₂. Finally, the algorithm includes an error analysis module which is
29 fully described here. We also discuss verification results (as part of the algorithm
30 development) and future validation needs of the TROPOMI SO₂ algorithm.

31



1

2 1. INTRODUCTION

3 Sulfur dioxide enters the Earth's atmosphere via both natural and anthropogenic processes.
4 Through the formation of sulfate aerosols and sulfuric acid, it plays an important role on the
5 chemistry at local and global scales and its impact ranges from short term pollution to
6 climate forcing. While about one third of the global sulfur emissions originates from natural
7 sources (volcanoes and biogenic dimethyl sulfide), the main contributor to the total budget
8 is from anthropogenic emissions mainly from the combustion of fossil fuels (coal and oil) and
9 from smelting. Over the last decades, a host of satellite-based UV-visible instruments have
10 been used for the monitoring of anthropogenic and volcanic SO₂ emissions. Total vertical
11 column density (VCD) of SO₂ has been retrieved with the sensors TOMS (Krueger, 1983),
12 GOME (Eisinger and Burrows, 1998; Thomas et al., 2005; Khokar et al., 2005), SCIAMACHY
13 (Afe et al., 2004), OMI (Krotkov et al., 2006; Yang et al., 2007, 2010; Li et al., 2013; Theys et
14 al., 2015), GOME-2 (Richter et al., 2009; Bobrowski et al., 2010; Nowlan et al., 2011; Rix et
15 al., 2012; Hörmann et al., 2013) and OMPS (Yang et al., 2013). In particular, the Ozone
16 Monitoring Instrument (OMI) has largely demonstrated the value of satellite UV-visible
17 remote-sensing (1) in monitoring volcanic plumes in near-real time (Brenot et al., 2014) and
18 changes in volcanic degassing at the global scale (Carn et al., 2016, and references therein),
19 (2) in detecting and quantifying large anthropogenic SO₂ emissions, weak or unreported
20 emission sources worldwide (Theys et al., 2015; Fioletov et al., 2016; McLinden et al., 2016)
21 as well as investigating their long-term changes (Krotkov et al., 2016; van der A et al., 2016).
22 An exemplary map of OMI SO₂ columns (Theys et al., 2015) averaged over the 2005-2009
23 period is shown in Figure 1, illustrating typical anthropogenic emission hotspots (China,
24 Eastern Europe, India and the Middle East) and signals from volcanic activity (e.g. from the
25 volcanoes in D.R. Congo).

26 The 7-year lifetime Sentinel-5p sensor TROPOMI (Veefkind et al., 2012) will fly on a polar low
27 earth orbit with a wide swath of 2600 km. The TROPOMI instrument is a push-broom
28 imaging spectrometer similar in concept as OMI. It has eight spectral bands covering UV to
29 SWIR wavelengths. The SO₂ retrieval algorithm exploits measurements from band 3 (310-405
30 nm), with typical spectral resolution of 0.54 nm, signal-to-noise ratio of about 1000 and pixel
31 size as good as 7x3.5 km².



1 TROPOMI will continue and improve the measurement time-series of OMI SO₂ and other UV
2 sensors. Owing to similar performance as OMI in terms of signal-to-noise ratio and
3 unprecedented spatial resolution, TROPOMI will arguably discern very fine details in the SO₂
4 distribution and will be able to detect point sources with annual SO₂ emissions of about 10
5 kT/year or lower (using oversampling techniques).

6 This paper gives a thorough description of the operational TROPOMI SO₂ algorithm and
7 reflects the S5P SO₂ L2 Algorithm Theoretical Basis Document v1.0. In Section 2, we first
8 present the product requirements and briefly discuss the expected product performance in
9 terms of precision and accuracy. It is then followed by the SO₂ column retrieval algorithm
10 description. An error analysis of the retrieval method is presented in Section 3. Results from
11 algorithm verification exercise using an independent retrieval scheme is given in Section 4.
12 The possibilities for future validation of the retrieved SO₂ data product can be found in
13 Section 5. Conclusions are given in Section 6. Additional information on data product and
14 auxiliary data are provided in annex.

15 **2. TROPOMI SO₂ ALGORITHM**

16 **2.1 PRODUCT REQUIREMENTS**

17 While UV measurements are highly sensitive to SO₂ at high altitudes (upper troposphere-
18 lower stratosphere), the sensitivity to SO₂ concentration in the boundary layer is intrinsically
19 limited from space due to the combined effect of scattering (Rayleigh and Mie) and ozone
20 absorption that hamper the penetration of solar radiation into the lowest atmospheric
21 layers. Furthermore the SO₂ absorption signature suffers from the interference with the
22 ozone absorption spectrum.

23 The retrieval precision (or random uncertainty) is driven by the signal to noise ratio of the
24 recorded spectra and by the retrieval wavelength interval used, the accuracy (or systematic
25 uncertainty) is limited by the knowledge on the auxiliary parameters needed in the different
26 retrieval steps. Among these are the treatment of other chemical interfering species, clouds
27 and aerosol, the representation of vertical profiles (gas, temperature, pressure), and
28 uncertainties on data from external sources (e.g., surface reflectance).



1 Requirements on the accuracy and precision for the data products derived from the
2 TROPOMI measurements are specified in the GMES Sentinels 4 and 5 and 5p Mission
3 Requirements Document MRD (Langen et al., 2011), the Report of The Review Of User
4 Requirements for Sentinels-4/5 (Bovensmann et al., 2011) and the Science Requirements
5 Document for TROPOMI (van Weele et al., 2008). These requirements derive from the
6 CAPACITY study (Kelder et al., 2005) and have been fine-tuned by the CAMELOT (Levelt et
7 al., 2009) and ONTRAQ (Zweers et al., 2010) studies. The CAPACITY study has defined three
8 main themes: The ozone layer (A), air quality (B), and climate (C) with further division into
9 sub themes. Requirements for SO₂ have been specified for a number of these sub themes. In
10 the following paragraphs, we discuss these requirements and the expected performances of
11 the SO₂ retrieval algorithm (summary is given in Table 1).

12 *Theme A3 - Ozone layer assessment*
13

14 This theme addresses the importance of measurements in the case of enhanced SO₂
15 concentrations in the stratosphere due to severe volcanic events. Long-term presence (up to
16 several months) of SO₂ in the stratosphere contributes to the stratospheric aerosol loading
17 and hence affects the climate and the stratospheric ozone budget. For such scenarios, the
18 requirements state that the stratospheric vertical column should be monitored with a total
19 uncertainty of 30%. Although powerful volcanic events generally produce large amounts of
20 SO₂, monitoring such a plume over extended periods of time requires the detection of the
21 plume also after it has diluted during the weeks after the eruption.



1 From an error analysis of the proposed SO₂ algorithm (Section 3), we have assessed the
2 major sources of uncertainty in the retrieved SO₂ column. One of the main contributors to
3 the total uncertainty is instrumental noise. This source of error alone limits the precision to
4 vertical columns above about 0.25 DU (1 DU=2.69 x 10¹⁶ molec.cm⁻²). For SO₂ in the
5 stratosphere, the summing up of the various uncertainties (Section 3) is believed to be
6 around the required uncertainty of 30% for diluted SO₂ plumes, provided that the vertical
7 column is larger than 0.5 DU. Explosive volcanic eruptions capable of injecting SO₂ into the
8 stratosphere regularly show stratospheric SO₂ columns of a few DU to several hundreds of
9 DU or more, as was the case, for example, for the eruptions of Mt. Kasatochi (Yang et al.,
10 2010) and Sarychev Peak (Carn et al., 2011). For very large SO₂ concentrations, the
11 dynamical use of different fitting windows (see section 2.2) enables to reach 30 %
12 uncertainty level.

13 *Theme B – Air quality*

14

15 This theme includes three sub themes:

16 B1 -Protocol monitoring: This involves the monitoring of abundances and concentrations
17 of atmospheric constituents, driven by several agreements, such as the Gothenburg
18 protocol, National Emission Ceilings, and EU Air Quality regulations.

19 B2 -Near-real time (NRT) data requirements: This comprises the relatively fast (~30
20 minutes) prediction and determination of surface concentrations in relation to health
21 and safety warnings.

22 B3 – Assessment: This sub theme aims at answering several air quality related scientific
23 questions, such as the effect on air quality of special and temporal variations in oxidizing
24 capacity and long-range transport of atmospheric constituents.

25 A more detailed description of the air quality sub themes can be found in Langen et al.
26 (2011).



1 The user requirements on SO₂ products are equal for all three sub themes. For the total
2 vertical column and the tropospheric vertical column of SO₂, the user requirements state an
3 absolute maximum uncertainty of 1.3×10^{15} molecules cm⁻² or 0.05 DU. This number derives
4 from the ESA CAPACITY study, where the number was expressed as 0.4 ppbv for a 1.5 km
5 thick boundary layer reaching up to 850 hPa. From the uncertainty due to instrument noise
6 only, it is clear that the 0.05 DU requirement cannot be met on a single-measurement basis.
7 This limitation was already found in the ESA CAMELOT study (Levelt et al., 2009).

8 For anthropogenic SO₂ typically confined in the planetary boundary layer (PBL), calculations
9 performed within the CAMELOT study showed that the smallest vertical column that can be
10 detected in the PBL is of about 1-3 DU (for a signal-to-noise ratio (SNR) of 1000). Although
11 pollution hotspots can be better identified by spatial or temporal averaging, several
12 uncertainties (e.g. due to varying surface albedo or SO₂ vertical profile shape) are not
13 averaging out and directly limit the product accuracy to about 50% or more. Though the
14 difference between the MRD requirements and the expected TROPOMI performance is
15 rather large, one could argue that the required threshold should not be a strict criterion in all
16 circumstances. The user requirement of 0.05 DU represents the maximum uncertainty to
17 distinguish (anthropogenic) pollution sources from background concentrations. Bovensmann
18 et al. (2011) reviewed the MRD user requirements and motivated a relaxation of certain user
19 requirements for specific conditions. For measurements in the PBL, the document proposes
20 a relative requirement of 30-60% in order to discriminate between enhanced (> 1.5 ppbv),
21 moderate (0.5-1.5 ppbv), and background concentrations (<0.5 ppbv). It is expected that it
22 will be possible to discriminate these three levels by averaging (spatially-temporally)
23 TROPOMI data.

24 For volcanic SO₂ plumes in the free-troposphere, a better measurement sensitivity is
25 expected for TROPOMI. The expected precision is about 0.5 DU on the vertical column. The
26 accuracy on the SO₂ vertical column will be strongly limited by the SO₂ plume height and the
27 cloud conditions. As these parameters are highly variable in practice, it is difficult to
28 ascertain the product accuracy for these conditions.

29
30
31



1 **2.2 ALGORITHM DESCRIPTION**

2 The first algorithm to retrieve SO₂ columns from space-borne UV measurements was
3 developed based on a few wavelength pairs (for TOMS) and has been subsequently applied
4 and refined for OMI measurements (e.g., Krotkov et al., 2006; Yang et al., 2007 and
5 references therein). Current algorithms exploit back-scattered radiance measurements in a
6 wide spectral range using a direct fitting approach (Yang et al., 2010; Nowlan et al., 2011), a
7 Principal Component Analysis (PCA) method (Li et al., 2013) or (some form of) Differential
8 Optical Absorption Spectroscopy (DOAS; Platt and Stutz, 2008), see e.g. Richter et al. (2009),
9 Hörmann et al. (2013), Theys et al. (2015).

10 Direct fitting schemes in which on-the-fly radiative transfer simulations are made for all
11 concerned wavelengths and resulting simulated spectra are adjusted to the spectral
12 observations, are in principle the most accurate. They are able to cope with very large SO₂
13 columns (such as those occurring during explosive volcanic eruptions), i.e. conditions
14 typically leading to a strongly non-linear relation between the SO₂ signal and the VCD.
15 However, the main disadvantage of direct fitting algorithms with respect to DOAS (or PCA), is
16 that they are computationally expensive and are out of reach for TROPOMI operational near-
17 real-time processing, for which the Level 1b data flow is expected to be massive and deliver
18 around 1,5 million spectral measurements per orbit (~15 orbits daily) for band 3 (with a
19 corresponding data size of 6 gigabytes). To reach the product accuracy and processing
20 performance requirements, the here adopted approach applies DOAS in three different
21 fitting windows (within the 310-390 nm spectral range) that are still sensitive enough to SO₂
22 but less affected by non-linear effects (Bobrowski et al., 2010; Hörmann et al., 2013).

23



1 Figure 2 shows the full flow diagram of the SO₂ retrieval algorithm including the
2 dependencies on auxiliary data and other L2 products. The algorithm and its application to
3 OMI data is also described in Theys et al. (2015), although there are differences in some
4 settings. The baseline operation flow of the scheme is based on a DOAS retrieval algorithm
5 and is identical to that implemented in the retrieval algorithm for HCHO (also developed by
6 BIRA-IASB, see De Smedt et al., 2016). The main output parameters of the algorithm are SO₂
7 vertical column density, slant column density, air mass factor, averaging kernels (AK) and
8 error estimates. Here, we will first briefly discuss the principle of the DOAS VCD retrieval
9 before discussing the individual steps of the process in more details.

10 First, the radiance and irradiance data are read from a S5P L1b file, along with geolocation
11 data such as pixel coordinates and observation geometry (sun and viewing angles). At this
12 stage also cloud cover information is obtained from the S5P cloud L2 data, as required for
13 the calculation of the AMF, later in the scheme. Then relevant absorption cross section data,
14 as well as characteristics of the instrument (e.g., slit functions) are used as input for the SO₂
15 slant column density determination. As a baseline, the slant column fit is done in a sensitive
16 window from 312 to 326 nm. For pixels with a strong SO₂ signal, results from alternative
17 windows, where the SO₂ absorption is weaker can be used instead. An empirical offset
18 correction (dependent on the fitting window used) is then applied to the SCD. The latter
19 correction accounts for systematic biases in the SCDs. Following the SCD determination, the
20 AMF is estimated based on a pre-calculated weighting functions (or box-AMFs) look-up table
21 (LUT). This look-up-table is generated using the Linearized Discrete Ordinate Radiative
22 Transfer (LIDORT) code (Spurr, 2008) and has several entries: cloud cover data, topographic
23 information, observation geometry, surface albedo, effective wavelength (representative of
24 the fitting window used), total ozone column and the shape of the vertical SO₂ profile. The
25 algorithm also includes an error calculation and retrieval characterization module (Section 3)
26 that computes the averaging kernels (Eskes & Boersma, 2003), which characterize the
27 vertical sensitivity of the measurement and which are required for comparison with other
28 types of data (Veefkind et al., 2012).

29 The final SO₂ vertical column is obtained by:

$$30 \quad N_v = \frac{N_s - N_s^{back}}{M} \quad (1)$$



1 where the main quantities are the vertical column (N_v), the slant column density (N_s) and the
2 values used for the background correction (N_s^{back}). M is the air mass factor.

3 **2.2.1 Slant column retrieval**

4 The backscattered radiance spectrum recorded by the space instrument differs from the
5 solar spectrum because of the interactions of the photons with the Earth's atmosphere and
6 surface reflection. Hence the reflectance spectra contains spectral features that can be
7 related to the various absorbing species and their amounts in the atmosphere. The DOAS
8 method aims at the separation of the highly structured trace gas absorption spectra and
9 broadband spectral structures. The technique relies on a number of assumptions that can be
10 summarized as follows:

- 11 a. The spectral analysis and atmospheric radiative transfer computations are treated
12 separately, by considering one averaged atmospheric light path of the photons
13 travelling from the sun to the instrument.
- 14 b. The absorption cross-sections are not strongly dependent on pressure and
15 temperature. Additionally, the averaged light path should be weakly dependent on
16 the wavelength - for the fitting window used - which enables to define an effective
17 absorption (slant) column density. It should be noted that strictly this is not valid for
18 the SO_2 DOAS retrieval because of strong absorption by ozone and in some cases SO_2
19 itself (for large SO_2 amounts).
- 20 c. Spectrally smoothed structures due broadband absorption, scattering and reflection
21 processes can be well reproduced by a low-order polynomial as a function of
22 wavelength.

23 Photons collected by the satellite instrument may have followed very different light paths
24 through the atmosphere depending on their scattering history. However, a single effective
25 light path is assumed, which represents an average of the complex paths of all reflected and
26 scattered solar photons reaching the instrument within the spectral interval used for the
27 retrieval. This simplification is valid if the effective light path is reasonably constant over the
28 considered wavelength range. The spectral analysis can be described by the following
29 equation:



$$\ln \frac{\pi I(\lambda)}{\mu_0 E_0(\lambda)} = - \sum_j \sigma_j(\lambda) N_{S_j} + \sum_p c_p \lambda^p \quad (2)$$

1 Here, $I(\lambda)$ is the observed backscattered Earthshine radiance [$\text{W m}^{-2}\text{nm}^{-1}\text{sr}^{-1}$], E_0 is the solar
2 irradiance [$\text{W m}^{-2}\text{nm}^{-1}$] and $\mu_0 = \cos \theta_0$. The first term on the right hand side indicates all
3 relevant absorbing species with absorption cross-sections σ_j [$\text{cm}^2 \text{molec.}^{-1}$]. Integration of
4 the number densities of these species along the effective light path gives the slant column
5 density N_{S_j} [molec.cm^{-2}]. Equation 2 can be solved by least-squares fitting techniques (Platt
6 and Stutz, 2008) for the slant column values. The final term in Eq. 2 is the polynomial
7 representing broad band absorption and (Rayleigh and Mie) scattering structures in the
8 observed spectrum and also accounts for possible errors such as e.g. uncorrected instrument
9 degradation effects, uncertainties in the radiometric calibration or possible residual
10 (smooth) polarization response effects not accounted for in the level 0-1 processing.

11 Apart from the cross-sections for the trace gases of interest, additional fit parameters need
12 to be introduced to account for the effect of several physical phenomena on the fit result.
13 For SO_2 fitting, these are the filling-in of Fraunhofer lines (Ring effect) and the need for an
14 intensity offset-correction. In the above, we have assumed that for the ensemble of
15 observed photons a single effective light path can be assumed over the adopted wavelength
16 fitting interval. For the observation of (generally small) SO_2 concentrations at large solar
17 zenith angles (SZA) this is not necessarily the case. For such long light paths, the large
18 contribution of O_3 absorption may lead to negative SO_2 retrievals. This may be mitigated by
19 taking the wavelength dependence of the O_3 SCD over the fitting window into account, as
20 will be described in the next section.

21 The different parts of the DOAS retrieval are detailed in the next subsections and Table 2
22 gives a summary of settings used to invert SO_2 slant columns. Note that in Eq. 2, the daily
23 solar irradiance is used as a baseline for the reference spectrum. As a better option, it is
24 generally preferred to use daily averaged radiances, selected for each across-track position,
25 in the equatorial Pacific. In the NRT algorithm, the last valid day can be used to derive the
26 reference spectra, while in the offline version of the algorithm, the current day should be
27 used. Based on OMI experience, it would allow e.g. for better handling of instrumental



1 artifacts and degradation of the recorded spectra for each detector. At the time of writing, it
2 is planned to test this option during the S5P commissioning phase.

3 2.2.1.1 Wavelength fitting windows

4
5 DOAS measurements are in principle applicable to all gases having suitable narrow
6 absorption bands in the UV, visible, or near IR regions. However, the generally low
7 concentrations of these compounds in the atmosphere, and the limited signal-to-noise ratio
8 of the spectrometers, restrict the number of trace gases that can be detected. Many spectral
9 regions contain several interfering absorbers and correlations between absorber cross-
10 sections can sometimes lead to systematic biases in the retrieved slant columns. In general,
11 the correlation between cross-sections decreases if the wavelength interval is extended, but
12 then the assumption of a single effective light path defined for the entire wavelength
13 interval may not be fully satisfied, leading to systematic misfit effects that may also
14 introduce biases in the retrieved slant columns (e.g., Pukītė et al., 2010). To optimize DOAS
15 retrieval settings, a trade-off has to be found between these effects. In the UV-visible
16 spectral region, the cross-section spectrum of SO₂ has its strongest bands in the 280-320 nm
17 range (Figure 3). For the short wavelengths in this range, the SO₂ signal however suffers
18 from a strong increase in Rayleigh scattering and ozone absorption. In practice, this leads to
19 a very small SO₂ signal in the satellite spectra compared to ozone absorption, especially for
20 tropospheric SO₂. Consequently, SO₂ is traditionally retrieved (for GOME, SCIAMACHY,
21 GOME-2, OMI) using sensitive windows in the 310-326 nm range. Note that even in this
22 range the SO₂ absorption can be three orders of magnitude lower than that of ozone.

23 The TROPOMI SO₂ algorithm is using a multiple windows approach:

- 24 • 312-326 nm: classical fitting window, ideal for small columns. This window is used as
25 baseline. If non-linear effects due to high SO₂ amounts are encountered, one of the
26 two following windows will be used instead.
- 27 • 325-335 nm: in this window, differential SO₂ spectral features are one order of
28 magnitude smaller than in the classical window. It allows the retrieval of moderate
29 SO₂ columns, an approach similar to the one described by Hörmann et al. (2013).



- 1 • 360-390 nm: SO₂ absorption bands are 2-3 orders of magnitude weaker than in the
2 classical window and are best suited for the retrieval of extremely high SO₂ columns
3 (Bobrowski et al., 2010)

4 Note that in the 325-335 nm and 360-390 nm windows the Rayleigh scattering and ozone
5 absorption are less important than in the baseline 312-326 nm window (see also Figure 3).

6 Specifically, in the first two intervals, absorption cross-sections of O₃ at 228K and 243K are
7 included in the fit and, to better cope with the strong (non-linear) ozone absorption at short
8 wavelengths, the retrieval also includes two pseudo cross-sections following the approach of
9 Puķīte et al. (2010): $\lambda\sigma_{O_3}$ and $\sigma_{O_3}^2$ calculated from the O₃ cross-section spectrum at 228K.
10 The correction for the Ring effect is based on the technique outlined by Vountas et al.
11 (1998). This technique involves a Principal Component Analysis of a set of Ring spectra,
12 calculated for a range of solar zenith angles. The first two of the resulting eigenvectors
13 appear to accurately describe the Ring spectra, with the first eigenvector representing the
14 filling-in of Fraunhofer lines and the second mostly representing the filling-in of gas
15 absorption features. In the retrieval algorithm, these vectors are determined by
16 orthogonalizing two Ring spectra, calculated by LIDORT-RRS (Spurr et al., 2008), a version of
17 LIDORT accounting for rotational Raman scattering, for a low SZA (20°) and a high SZA (87°),
18 respectively.

19 2.2.1.2 Wavelength calibration and convolution to TROPOMI resolution

20 The quality of a DOAS fit critically depends on the accuracy of the alignment between the
21 earthshine radiance spectrum, the reference spectrum and the cross-sections. Although the
22 Level 1b will contain a spectral assignment, an additional spectral calibration is part of the
23 SO₂ algorithm. Moreover, the DOAS spectral analysis includes also the fit of shift and stretch
24 of radiance spectra because the TROPOMI spectral registration will differ from one ground-
25 pixel to another e.g. due to thermal variations over the orbit as well as due to
26 inhomogeneous filling of the slit in flight direction.

27 The wavelength registration of the reference spectrum can be fine-tuned by means of a
28 calibration procedure making use of the solar Fraunhofer lines. To this end, a reference solar
29 atlas E_s accurate in absolute vacuum wavelength to better than 0.001 nm (Chance and



1 Kurucz, 2010) is degraded at the resolution of the instrument, through convolution by the
2 TROPOMI instrumental slit function.

3 Using a non-linear least-squares approach, the shift (Δ_i) between the reference solar atlas
4 and the TROPOMI irradiance is determined in a set of equally spaced sub-intervals covering a
5 spectral range large enough to encompass all relevant fitting intervals. The shift is derived
6 according to the following equation:

$$E_0(\lambda) = E_s(\lambda - \Delta_i) \quad (3)$$

7 where E_s is the solar spectrum convolved at the resolution of the instrument and Δ_i is the
8 shift in sub-interval i . A polynomial is then fitted through the individual points in order to
9 reconstruct an accurate wavelength calibration $\Delta(\lambda)$ for the complete analysis interval. Note
10 that this approach allows to compensate for stretch and shift errors in the original
11 wavelength assignment.

12 In the case of TROPOMI, the procedure is complicated by the fact that such calibrations must
13 be performed (and stored) for each separate spectral field on the CCD detector array. Indeed
14 due to the imperfect characteristics of the imaging optics, each row of the TROPOMI
15 instrument must be considered as a separate spectrometer for analysis purposes.

16 In a subsequent step of the processing, the absorption cross-sections of the different trace
17 gases must be convolved with the instrumental slit function. The baseline approach is to use
18 slit functions determined as part of the TROPOMI key data. Slit functions are delivered for
19 each binned spectrum and as a function of wavelength. Note that an additional feature of
20 the prototype algorithm allows to dynamically fit for an effective slit function of known line
21 shape (e.g. asymmetric Gaussian). This can be used for verification and monitoring purpose
22 during commissioning and later on during the mission.

23 More specifically, wavelength calibrations are made for each TROPOMI orbit as follows:

- 24 1. The TROPOMI irradiances (one for each row of the CCD) are calibrated in wavelength
25 over the 310-390 nm wavelength range, using 10 sub-windows.
- 26 2. The earthshine radiances and the absorption cross-sections are interpolated (cubic
27 spline interpolation) on the calibrated wavelength grid, prior to the analysis.



1 3. During spectral fitting, shift and stretch parameters are further derived to align
2 radiance and irradiance spectra. The reference wavelength grid used in the DOAS
3 procedure is the (optimized) grid of the TROPOMI solar irradiance.

4 2.2.1.3 Spike removal algorithm

5
6 A method to remove individual hot pixels or pixels affected by the South Atlantic Anomaly
7 has been presented for NO₂ retrievals in Richter et al. (2011). Often only a few individual
8 detector pixels are affected and in these cases, it is possible to identify and remove the noisy
9 points from the fit. However, as the amplitude of the distortion is usually only of the order of
10 a few percent or less, it cannot always be found in the highly structured spectra themselves.
11 Higher sensitivity for spikes can be achieved by analysing the residual of the fit where the
12 contribution of the Fraunhofer lines, scattering, and absorption is already removed.

13 When the residual for a single pixel exceeds the average residual of all pixels by a chosen
14 threshold ratio (the tolerance factor), the pixel is excluded from the analysis, in an iterative
15 process. This procedure is repeated until no further outliers are identified, or until the
16 maximum number of iterations is reached (here fixed to 3). This is especially important to
17 handle the degradation of 2-D detector arrays such as OMI or TROPOMI. However, this
18 improvement of the algorithm has a non-negligible impact on the time of processing. At the
19 time of writing, the exact values for the tolerance factor and maximum number of iterations
20 of the spike removal procedure are difficult to ascertain and will only be known during
21 operations. To assess the impact on the processing time, test retrievals have been done on
22 OMI spectra using a tolerance factor of 5, and a limit of 3 iterations (this could be relaxed)
23 and it leads to an increase in processing time by a factor of 1.5.

24

25

26

27



1 2.2.1.4 Fitting window selection

2

3 The implementation of the multiple fitting windows retrieval requires selection criteria for
4 the transition from one window to another. These criteria are based on the measured SO₂
5 slant columns. As a baseline, the SO₂ SCD in the 312-326 nm window will be retrieved for
6 each satellite pixel. When the resulting value exceeds a certain criterion, the slant column
7 retrieval is taken from an alternative window. As part of the algorithm development and
8 during the verification exercise (Section 4), closed-loop retrievals have been performed and
9 application of the algorithm to real data from the GOME-2 and OMI instruments lead to
10 threshold values and criteria as given in Table 3.

11 **2.2.2 Offset correction**

12 When applying the algorithm to OMI and GOME-2 data, across-track/viewing angle
13 dependent residuals of SO₂ were found over clean areas and negative SO₂ SCDs are found at
14 high SZA which need to be corrected (note that this is a common problem of most
15 algorithms to retrieve SO₂ from space UV sensors). A background correction scheme was
16 found mostly necessary for the SO₂ slant columns retrieved in the baseline fitting window.
17 The adopted correction scheme depends on across-track position and measured O₃ slant
18 column as described below.

19 The correction is based on a parameterization of the background values that are then
20 subtracted from the measurements. The scheme first removes pixels with high SZA (>70°) or
21 SCDs larger than 1.5 DU (measurements with presumably real SO₂) and then calculates the
22 offset correction by averaging the SO₂ data on an ozone slant column grid (bins of 75 DU).
23 This is done independently for each across-track position and hemisphere, and the
24 correction makes use of measurements averaged over a time period of two weeks preceding
25 the measurement of interest (to improve the statistics and minimize the impact of a possible
26 extended volcanic SO₂ plume on the averaged values).

27 It should be noted that the O₃ slant column is dependent on the wavelength when applying
28 the approach of Pukite et al. (2010):

29
$$SCD(\lambda) = SCD_{T1} + SCD_{T2} + \lambda \cdot SCD_{\lambda} + \sigma_s(\lambda) SCD_S \quad (4)$$



1 SCD_{T1} and SCD_{T2} are the retrieved ozone slant columns corresponding to the ozone cross-
2 sections at two temperatures (T1, T2) included in the fit. SCD_λ and SCD_σ are the retrieved
3 parameters for the two pseudo cross-sections $\lambda \cdot \sigma_s$ and σ_s^2 (σ_s being the O₃ cross-section at
4 T1). In order to apply the background correction, the O₃ slant column expression (Eq. 4) is
5 evaluated at 313 nm (read below).

6 An example of the effect of the background correction is shown in Figure 4 for OMI. One can
7 see that after correction (top panel) the retrievals show smooth/unstriped results and values
8 close to zero outside the polluted areas. In some regions (in particular at high latitudes),
9 residual columns can be found, but are generally lower than 0.2 DU.

10 For the two additional fitting windows, residual SO₂ levels are relatively small in comparison
11 to the column amounts expected to be retrieved in these windows. However, simplified
12 background corrections are also applied to the alternative windows: the offset corrections
13 use parameterizations of the background slant columns based on latitude (bins of 5°), cross-
14 track position and time (two weeks moving averages as for the baseline window). To avoid
15 contamination by strong volcanic eruptions, only the pixels are kept with SCD less than 50DU
16 and 250DU for the fitting windows 325-335nm and 360-390nm, respectively.

17 It should be noted that the background corrections do not imply to save two weeks of SO₂ L2
18 data in intermediate products, but only the averaged values ($\sum_{i=1,N} \text{SCD}_i / N$) over the
19 predefined working grids (note: the numerators $\sum_{i=1,N} \text{SCD}_i$ and denominators N are stored
20 separately).

21 This background correction is well suited for the case of a 2D-detector array such as
22 TROPOMI, for which across-track striping can possibly arise due to imperfect cross-
23 calibration and different dead/hot pixel masks for the CCD detector regions. This
24 instrumental effect can also be found for scanning spectrometers, but since these
25 instruments only have one single detector, such errors do not appear as stripes. These
26 different retrieval artefacts can be compensated (up to a certain extent) using background
27 corrections which depend on the across-track position. All of these corrections are also
28 meant to handle the time-dependent degradation of the instrument. Note that experiences
29 with OMI show that the most efficient method to avoid across-track stripes in the retrievals
30 is to use row-dependent mean radiances as control spectrum in the DOAS fit.



1 2.2.3 Air mass factors

2 The DOAS method assumes that the retrieved slant column (after appropriate background
3 correction) can be converted into a vertical columns using a single air mass factor M
4 (representative for the fitting interval):

$$M = \frac{N_s}{N_v} \quad (5)$$

5 which is determined by radiative transfer calculations with LIDORT version 3.3 (Spurr, 2008).

6 The AMF calculation is based on the formulation of Palmer et al. (2001):

$$M = \int m'(p) \cdot s(p) dp \quad (6)$$

7 with $m'=m(p)/C_{temp}(p)$, where $m(p)$ is the so-called weighting function (WF) or pressure
8 dependent air mass factor, C_{temp} is a temperature correction (see section 2.2.3.7) and s is the
9 SO₂ normalized a-priori mixing ratio profile, as function of pressure (p).

10 The AMF calculation assumes Lambertian reflectors for the ground and the clouds and
11 makes use of pre-calculated WF LUTs at 313, 326 and 375 nm (depending on the fitting
12 window used). Calculating the AMF at these three wavelengths was found to give the best
13 results using closed-loop retrievals (see Auxiliary material of Theys et al., 2015). The WF
14 depends on observation geometry (solar zenith angle: SZA, line-of-sight angle: LOS, relative
15 azimuth angle: RAA), total ozone column (TO3), scene albedo (alb), surface pressure (p_s),
16 cloud top pressure (p_{cloud}) and effective cloud fraction (f_c).

17 Examples of SO₂ weighting functions are displayed in Figure 5 (as a function of height for
18 illustration purpose) and show the typical variations of the measurement sensitivity as a
19 function of height, wavelength and surface albedo.

20 The generation of the WF LUT has been done for a large range of physical parameters, listed
21 in Table 4. In practice, the WF for each pixel is computed by linear interpolation of the WF
22 LUT at the a-priori profile pressure grid and using the auxiliary data sets described in the
23 following sub-sections. Linear interpolations are performed along the cosine of solar and
24 viewing angles, relative azimuth angle and surface albedo, while a nearest neighbor
25 interpolation is performed in surface pressure. In particular, the grid of surface pressure is
26 very thin near the ground, in order to minimize interpolation errors caused by the generally



1 low albedo of ground surfaces. Furthermore, the LUT and model pressures are scaled to the
2 respective surface pressures, in order to avoid extrapolations outside the LUT range.

3 2.2.3.1 Observation geometry

4 The LUT covers the full range of values for solar zenith angles, line-of-sight angles and
5 relative azimuth angles that can be encountered in the TROPOMI measurements. The
6 observation geometry is readily present in the L1b data for each satellite pixel.

7 2.2.3.2 Total ozone column

8 The measurement sensitivity at 313 nm is dependent on the total ozone absorption. The LUT
9 covers a range of ozone column values from 200 to 500 DU for a set of typical ozone profiles.
10 The total ozone column is directly available from the operational processing of the S5P total
11 ozone column product.

12 2.2.3.3 Surface albedo

13 For the surface albedo dimension, we use the climatological monthly minimum Lambertian
14 equivalent reflector (minLER) data from Kleipool et al. (2008) at 328 nm for w1 and w2, and
15 376 nm for w3. This database is based on OMI measurements and has a spatial resolution of
16 0.5° x 0.5°. The albedo value is very important for PBL anthropogenic SO₂ but less critical for
17 volcanic SO₂ when it is higher in the atmosphere.

18 2.2.3.4 Clouds

19 The AMF calculations for TROPOMI partly cloudy scenes use the cloud parameters (cloud
20 fraction, cloud albedo, cloud pressure) supplied by the nominal S5P cloud algorithm
21 OCRA/ROCINN in its Clouds as Reflecting Boundaries (CRB) implementation (Loyola et al.,
22 2016). The cloud surface is considered to be a Lambertian reflecting surface and the
23 treatment of clouds is achieved through the independent pixel approximation (IPA; Martin et
24 al., 2002) which considers a inhomogeneous satellite pixel as being composed (as for the
25 radiance intensity) of two independent homogeneous scenes, one completely clear and the
26 other completely cloudy. The weighting function is expressed as:

$$m(p) = \Phi m_{\text{cloud}}(p) + (1 - \Phi) m_{\text{clear}}(p) \quad (7)$$

27 where Φ is the intensity-weighted cloud fraction or cloud radiance fraction:



$$\Phi = \frac{f_c I_{cloud}}{f_c I_{cloud} + (1 - f_c) I_{clear}} \quad (8)$$

1 The suffixes clear and cloudy refer to the WF and intensity calculation corresponding to a
2 fully clear or cloudy pixel, respectively. The WF LUT is therefore accompanied by an intensity
3 LUT with the same input grids. Both LUTs have been generated for a range of cloud cover
4 fractions and cloud top pressures.

5 Note that the variations of the cloud albedo are directly related to the cloud optical
6 thickness. Strictly speaking, in a Lambertian (reflective) cloud model approach, only thick
7 clouds can be represented. An effective cloud fraction corresponding to an effective cloud
8 albedo of 0.8 ($f_{eff} \cong f_c \frac{A_c}{0.8}$) can be defined, in order to transform optically thin clouds into
9 equivalent optically thick clouds of reduced extent. Note that in some cases (thick clouds
10 with $A_c > 0.8$) the effective cloud fraction can be larger than one and the algorithm assumes
11 $f_{eff} = 1$. In such altitude dependent air mass factor calculations, a single cloud top pressure is
12 assumed within a given viewing scene. For low effective cloud fractions (f_{eff} lower than
13 10%), the current cloud top pressure output is highly unstable and it is therefore reasonable
14 to consider the observation as a clear-sky pixel (i.e. the cloud fraction is set to 0 in Eq. 8) in
15 order to avoid unnecessary error propagation through the retrievals, which can be as high as
16 100%. Moreover, it has been shown recently by Wang et al. (2016) using multi-axis DOAS
17 (MAX-DOAS) observations to validate satellite data that in case of elevated aerosol loadings
18 in the PBL (typically leading to apparent f_{eff} up to 10%), it is recommended to apply clear-
19 sky AMFs rather than total AMFs (based on cloud parameters) that presumably correct
20 implicitly for the aerosol effect on the measurement sensitivity.

21



1 It should be noted that the formulation of the pressure dependent air mass factor for a
2 partly cloudy pixel implicitly includes a correction for the SO₂ column lying below the cloud
3 and therefore not seen by the satellite, the so-called ghost column. Indeed, the total AMF
4 calculation as expressed by Eqs. 6 and 7 assumes the same shape factor and implies an
5 integration of the a-priori profile from the top of atmosphere to the ground, for each
6 fraction of the scene. The ghost column information is thus coming from the a-priori profile
7 shapes. For this reason, only observations with moderate cloud fractions (f_{eff} lower than
8 30%) are used, unless it can be assumed that the cloud cover is mostly situated below the
9 SO₂ layer, i.e. a typical situation for volcanic plumes injected in the upper-troposphere or
10 lower-stratosphere.

11 2.2.3.5 Surface height

12 The surface height (z_s) is determined for each pixel by interpolating the values of a high
13 resolution digital elevation map, GMTED2010 (Danielson et al., 2011).
14

15 2.2.3.6 Profile shapes

16 It is generally not possible to know at the time of observation what is the SO₂ vertical profile
17 and whether the observed SO₂ is of volcanic origin or from pollution (or both). Therefore, the
18 algorithm computes four vertical columns for different hypothetical SO₂ profiles.

19 Three box profiles of 1 km thickness, located in the boundary layer, upper-troposphere and
20 lower-stratosphere, are used. The first box profile stands for typical conditions of well mixed
21 SO₂ (from volcanic or anthropogenic emissions) in the boundary layer while the upper-
22 troposphere and lower stratosphere box profiles are representative of volcanic SO₂ plumes
23 from effusive and explosive eruptions, respectively.

24 In order to have more realistic SO₂ profiles for polluted scenes, daily forecasts calculated
25 with the global TM5 chemical transport model (Huijnen et al., 2010) will be used. TM5 will
26 be operated with a spatial resolution of 1°x1° in latitude and longitude, and with 34 sigma
27 pressure levels up to 0.1 hPa in the vertical direction. TM5 will use 3-hourly meteorological
28 fields from the European Centre for Medium Range Weather Forecast (ECMWF) operational
29 model (ERA-Interim reanalysis data for reprocessing, and the operational archive for real
30 time applications and forecasts). These fields include global distributions of wind,
31 temperature, surface pressure, humidity, (liquid and ice) water content, and precipitation. A



1 more detailed description of the TM5 model is given at <http://tm.knmi.nl/> and by van Geffen
2 et al. (2016).

3 For the calculation of the air mass factors, the profiles are linearly interpolated in space and
4 time, at the pixel centre and S5P local overpass time, through a model time step of 30
5 minutes. For NRT processing, the daily forecast of the TM5 model (located at KNMI) will be
6 ingested by the UPAS operational processor.

7 To reduce the errors associated to topography and the lower spatial resolution of the model
8 compared to the TROPOMI 7x3.5 km² spatial resolution, the a-priori profiles need to be
9 rescaled to effective surface elevation of the satellite pixel. The TM5 surface pressure is
10 converted by applying the hypsometric equation and the assumption that temperature
11 changes linearly with height (Zhou et al., 2009):

$$p_s = p_{TM5} \left(\frac{T_{TM5}}{T_{TM5} + \Gamma(z_{TM5} - z_s)} \right)^{-\frac{g}{R\Gamma}} \quad (9)$$

12 where p_{TM5} and T_{TM5} are the TM5 surface pressure and temperature, $\Gamma = 6.5\text{Kkm}^{-1}$ the
13 lapse rate, z_{TM5} the TM5 terrain height, and z_s surface elevation for the satellite ground
14 pixel.

15 2.2.3.7 Temperature correction

16 The SO₂ absorption cross-sections of Bogumil et al. (2003) show a clear temperature
17 dependence which has an impact on the retrieved SO₂ SCDs depending on the fitting
18 window used. However, only one temperature (203K) is used for the DOAS fit, therefore a
19 temperature correction needs to be applied: $\text{SCD}' = C_{\text{temp}} \cdot \text{SCD}$. While the SO₂ algorithm
20 provides vertical column results for a set of a-priori profiles, applying this correction to the
21 slant column is not simple and as a workaround it is preferred to apply the correction
22 directly to the AMFs (or box-AMFs to be precise) while keeping the (retrieved) SCD
23 unchanged: $\text{AMF}' = \text{AMF} / C_{\text{temp}}$. This formulation implicitly assumes that the AMF is not
24 strongly affected by temperature, which is a reasonable approximation (optically thin
25 atmosphere). The correction to be applied requires a temperature profile for each pixel
26 (which is obtained from the TM5 model):



1
$$C_{temp} = 1/[1 - \alpha \cdot (T[K] - 203)] \quad (10)$$

2 where α equals 0.002, 0.0038 and 0, for the fitting windows 312-326 nm, 325-335 nm and
3 360-390 nm, respectively. The parameter α has been determined empirically by fitting Eq. 10
4 through a set of data points (Figure 6), for each fitting window. Each value in Figure 6 is the
5 slope of the fitting line between the SO₂ differential cross-sections at 203K vs the cross-
6 section at a given temperature. In the fitting window 360-390 nm, no temperature
7 correction is applied ($\alpha=0$) because the cross-sections are quite uncertain. Moreover, the
8 360-390 nm wavelength range is meant for extreme cases (strong volcanic eruptions) for SO₂
9 plumes in the lower-stratosphere where a temperature of 203K is a good baseline.

10 2.2.3.8 Aerosols

11 The presence of aerosol in the observed scene (likely when observing anthropogenic
12 pollution or volcanic events), may affect the quality of the SO₂ retrieval (e.g. Yang et al.,
13 2010). No explicit treatment of aerosols (absorbing or not) is foreseen in the algorithm as
14 there is no general and easy way to treat the aerosols effect on the retrieval. At processing
15 time, the aerosol parameters (e.g., extinction profile or single scattering albedo) are
16 unknown. However, the information on the S5P UV Absorbing Aerosol Index (AAI) by Zweers
17 et al. (2016) will be included in the L2 SO₂ files as it gives information to the users on the
18 presence of aerosols both for anthropogenic and volcanic SO₂. Nevertheless, the AAI data
19 should be used/interpreted with care. In an offline future version of the SO₂ product,
20 absorbing aerosols might be included in the forward model, if reliable information on
21 absorbing aerosol can be obtained from the AAI and the S5P aerosol height product (Sanders
22 et al., 2016).

23

24

25

26

27

28

29



1 3. ERROR ANALYSIS

2 3.1 INTRODUCTION

3 The total uncertainty (accuracy and precision) on the SO₂ columns produced by the
4 algorithm presented in section 2, is composed of many sources of error (see also e.g., Lee et
5 al., 2009). Several of them are related to the instrument, such as uncertainties due to noise
6 or knowledge of the slit function. These instrumental errors propagate into the uncertainty
7 on the slant column. Other types of error can be considered as model errors and are related
8 to the representation of the physics in the algorithm. Examples of model errors are
9 uncertainties on the trace gas absorption cross-sections and the treatment of clouds. Model
10 errors can affect the slant column results or the air mass factors.

11 The total retrieval uncertainty on the SO₂ vertical columns can be derived by error
12 propagation, starting from Eq. 1 and if one assumes uncorrelated retrieval steps (Boersma et
13 al., 2004; De Smedt et al., 2008):

$$\sigma_{N_V}^2 = \left(\frac{\sigma_{N_S}}{M}\right)^2 + \left(\frac{\sigma_{N_S^{\text{back}}}}{M}\right)^2 + \left(\frac{(N_S - N_S^{\text{back}})\sigma_M}{M^2}\right)^2 \quad (11)$$

14 where σ_{N_S} and $\sigma_{N_S^{\text{back}}}$ are the errors on the slant column N_S and on the background correction
15 N_S^{back} , respectively.

16 The error analysis is complemented by the total column averaging kernel (AK) as described in
17 Eskes and Boersma (2003):

$$AK(p) = \frac{m'(p)}{M} \quad (12)$$

18 which is often used to characterize the sensitivity of the retrieved column to a change in
19 the true profile.

20 3.2 ERROR COMPONENTS

21 The following sections describe and characterize 20 error contributions to the total SO₂
22 vertical column uncertainty. These different error components and corresponding typical
23 values are summarized in Tables 5 and 6. Note that, at the time of writing, the precise effect
24 of several S5P-specific error sources are unknown and will be estimated during operations.



1 A difficulty in the error formulation presented above comes from the fact that it assumes the
2 different error sources/steps of the algorithm to be independent and uncorrelated, which is
3 not strictly valid. For example, the background correction is designed to overcome
4 systematic features/deficiencies of the DOAS slant column fitting and these two steps
5 cannot be considered as independent. Hence, summing up all the corresponding error
6 estimates would lead to overestimated error bars. Therefore, several error sources will be
7 discussed in the following sub-sections without giving actual values at this point. Their
8 impact is included and described in later sub-sections.

9 Another important point to note is that one should also (be able to) discriminate systematic
10 and random components of a given error source V :

$$11 \quad \sigma_V^2 = \frac{\sigma_{V(rand)}^2}{n} + \sigma_{V(syst)}^2 \quad (13)$$

12 here n is the number of pixels considered. However, they are hard to separate in practice.
13 Therefore, each of the 20 error contributions are (tentatively) classified as either “random”
14 or “systematic” errors, depending on their tendencies to average out in space/time or not.

15 **3.2.1 Errors on the slant column**

16 Error sources that contribute to the total uncertainty on the slant column originate both
17 from instrument characteristics and uncertainties/limitations on the representation of the
18 physics in the DOAS slant column fitting algorithm. For the systematic errors on the slant
19 column, the numbers provided in Table 5 have been determined based on sensitivity tests
20 (using the QDOAS software).

21 All effects summed in quadrature, the various contributions are estimated to account for a
22 systematic error of about 20% +0.2DU of the background-corrected slant column ($\sigma_{N_s, syst} =$
23 $0.2 * (N_s - N_s^{back}) + 0.2DU$).

24 For the random component of the slant column errors, the error on the slant columns
25 provided by the DOAS fit is considered (hereafter referred to as SCDE) as it is assumed to be
26 dominated by and representative for the different random sources of error.

27 *Error source 1: SO₂ cross-section*



1 Systematic errors on slant columns due to SO₂ cross-sections uncertainties are estimated to
2 be around 6% (Vandaele et al., 2009) in window 1 (312-326 nm) and window 2 (325-335 nm)
3 and unknown in window 3 (360-390 nm). In addition, the effect of the temperature on the
4 SO₂ cross-sections has to be considered as well. We refer to see section 3.2.2 for a discussion
5 of this source of error.

6 *Error source 2: O₃ and SO₂ absorption*

7 Non-linear effects due to O₃ absorption are to a large extent accounted for using the Taylor
8 expansion of the O₃ optical depth (Pukite et al., 2010). Remaining systematic biases are then
9 removed using the background correction; hence residual systematic features are believed
10 to be small (please read also the discussion on errors 9 and 10). The random component of
11 the slant column error contributes to SCDE.

12 Non-linear effects due to SO₂ absorption itself (mostly for volcanic plumes) are largely
13 handled by the triple windows retrievals but - as will be discussed in section 4 - the transition
14 between the different fitting windows is a compromise and there are cases where saturation
15 can still lead to rather large uncertainties. However, those are difficult to assess on a pixel to
16 pixel basis.

17 *Error source 3: Other atmospheric absorption/interferences*

18 In some geographical regions, several systematic features in the slant columns remain after
19 the background correction procedure (see discussion on error 9: background correction
20 error) and are attributed to spectral interferences not fully accounted for in the DOAS
21 analysis, such as incomplete treatment of the Ring effect. This effect has also a random
22 component and contributes to the retrieved SCD error (SCDE).

23 *Error source 4 : Radiance shot noise*

24 It has a major contribution to the SCDE and it can be estimated from typical S/N values of
25 S5P in UV band 3 (800-1000, according to Veefkind et al., 2012). This translates to typical
26 SCD random errors of about 0.3-0.5, 5 and 60 DU for window 1, 2 and 3, respectively. Note
27 that real measurements are needed to consolidate these numbers.

28 *Error source 5 : DOAS settings*



1 Tests on the effect of changing the lower and upper limits of the fitting windows by 1 nm
2 and the order of the closure polynomial (4 instead of 5) have been performed. Based on a
3 selection of orbits for the Kasatochi eruption (wide range of measured SCDs), the
4 corresponding SCD errors are less than 11, 6 and 8 % for window 1, 2 and 3, respectively.

5 *Error source 6: Wavelength and radiometric calibration*

6 Tests on the effect of uncertainties in the wavelength calibration have been performed in
7 the ESA CAMELOT study. The numbers are for a shift of 1/20th of the spectral sampling in
8 the solar spectrum and 1/100th of the spectral sampling in the Earthshine spectrum. The
9 shift can be corrected for, but interpolation errors can still lead to a remaining uncertainty of
10 a few percent.

11 Regarding radiometric calibration, the retrieval result is in principle insensitive to flat
12 (spectrally constant) offsets on the measured radiance because the algorithm includes an
13 intensity offset correction. From the ESA ONTRAQ study it was found that additive error
14 signals should remain within 2% of the measured spectrum.

15 *Error source 7: Spectral response function*

16 Uncertainties in the S5P instrumental slit functions can lead to systematic errors on the
17 retrieved SO₂ slant columns (to be determined).

18 *Error source 8: Other spectral features*

19 When additional spectral features of unknown origin are present in the measured spectrum,
20 the impact on the retrieved slant column values can be considerable. In the ONTRAQ study,
21 testing sinusoidal perturbation signals showed that this effect on the retrieval result
22 depends strongly on the frequency of the signal. Additives signals with an amplitude of 0.05
23 % of the measurement affect the retrieved SO₂ slant column up to 30%. The effect scales
24 more or less linearly with the signal amplitude.

25 *Error source 9: Background/destriping correction*

26 This error source is mostly systematic and important for anthropogenic SO₂ or for
27 monitoring degassing volcanoes. Based on OMI and GOME-2 test retrievals, the uncertainty
28 on the background correction is estimated to be < 0.2 DU. This value accounts for limitations



1 of the background correction in some clean areas (e.g. above the Sahara) where residual
2 slant columns values are typically found (after correction), or for a possible contamination by
3 volcanic SO₂, after a strong eruption.

4 **3.2.2 Errors on the air mass factor**

5 The error estimates on the AMF are listed in Table 6 and are based on simulations and
6 closed-loop tests using the radiative transfer code LIDORT. One can identify two sources of
7 errors on the AMF. First, the adopted LUT approach has limitations in reproducing the
8 radiative transfer in the atmosphere (forward model errors). Secondly, the error on the AMF
9 depends on input parameter uncertainties. This contribution can be broken down into a
10 squared sum of terms (Boersma et al., 2004):

$$\sigma_M^2 = \left(\frac{\partial M}{\partial \text{alb}} \cdot \sigma_{\text{alb}} \right)^2 + \left(\frac{\partial M}{\partial \text{ctp}} \cdot \sigma_{\text{ctp}} \right)^2 + \left(\frac{\partial M}{\partial f_c} \cdot \sigma_{f_c} \right)^2 + \left(\frac{\partial M}{\partial s} \cdot \sigma_s \right)^2 \quad (14)$$

11 where σ_{alb} , σ_{ctp} , σ_f , σ_s are typical uncertainties on the albedo, cloud top pressure, cloud
12 fraction and profile shape, respectively.

13 The contribution of each parameter to the total air mass factor error depends on the
14 observation conditions. The air mass factor sensitivities $\left(\frac{\partial M}{\partial \text{parameter}} \right)$, i.e. the air mass factor
15 derivatives with respect to the different input parameters, can be derived for any particular
16 condition of observation using the altitude-dependent AMF LUT, created with LIDORTv3.3,
17 and using the a-priori profile shapes. In practice, a LUT of AMF sensitivities has been created
18 using reduced grids from the AMF LUT and a parameterization of the profile shapes based on
19 the profile shape height.

20

21

22

23

24

25

26



1 *Error source 10: AMF wavelength dependence*

2 Because of strong atmospheric absorbers (mostly ozone) and scattering processes, the SO₂
3 AMF shows a wavelength dependence. We have conducted sensitivity tests to determine the
4 optimal wavelengths for AMF calculations representative for each of the three fitting
5 windows. To do so, synthetic radiances and SO₂ SCDs have been generated using LIDORT for
6 typical observations scenarios and at spectral resolution and sampling compatible with S5P.
7 The spectra have been analyzed by DOAS and the retrieved SCDs have been compared to the
8 calculated SCDs at different wavelengths. It comes out of this exercise that 313, 326 and 375
9 nm provide the best results, for window 1, 2 and 3, respectively. Figure 7 shows an
10 illustration of these sensitivity tests in the baseline window; an excellent correlation and
11 slope close to 1 is found for the scatter plot of retrieved versus simulated slant columns
12 using an effective wavelength of 313 nm for the AMF. Overall, for low solar zenith angles,
13 the deviations from the truth are less than 5% in most cases, except for boundary layer (BL)
14 SO₂ at a 1 DU column level and for low albedo scenes (deviations up to 20%). For high solar
15 zenith angles deviations are less than 10% in most cases, except for BL SO₂ at a 1 DU column
16 level and for low albedo scenes (underestimation up to a factor of 2).

17 *Error source 11: Model atmosphere*

18 This error relates to uncertainties in the atmospheric profiles used as input of LIDORT for the
19 weighting function look-up-table calculations.

20 Although the effect of O₃ absorption on the AMF is treated in the algorithm, the O₃ profiles
21 used as input of LIDORT are not fully representative of the real profiles and typical errors
22 (including error due to interpolation) of 5-10% can occur.

23 A test has been performed by replacing the US standard atmosphere pressure and
24 temperature profiles by high latitude winter profiles and the impact on the results is found
25 to be small.

26 *Error source 12 : Radiative transfer model*

27 It is believed to be small, less than 5% (Hendrick et al., 2006; Wagner et al., 2007).

28 *Error source 13 : Surface albedo*



1 A typical uncertainty on the albedo is 0.02 (Kleipool et al., 2008). This translates to an error
2 on the air mass factor after multiplication by the slope of the air mass factor as a function of
3 the albedo (Eq. 14) and can be evaluated for each satellite pixel. As an illustration, Figure 8
4 shows the expected dependence of the AMF with albedo and also with the cloud conditions.
5 From Figure 8a, one concludes that the retrievals of SO₂ in the BL are much more sensitive to
6 the exact albedo value than for SO₂ higher up in the atmosphere, for this particular example.

7 More substantial errors can be introduced if the real albedo differs considerably from what
8 is expected, for example in the case of the sudden snowfall or ice cover. The snow/ice cover
9 flag in the L2 file will therefore be useful for such cases.

10 *Error source 14: Cloud fraction*

11 An uncertainty on the cloud fraction of 0.05 is considered. The corresponding AMF error can
12 be estimated through Eq.14 (see Figure 8b) or by analytic derivation from Eqs. 6-8.

13 *Error source 15: Cloud top pressure*

14 An uncertainty on the cloud top height of 0.5 km (~50 hPa) is assumed. The corresponding
15 AMF error can be estimated through Eq. 14. Figure 8c illustrates the typical behaviour of
16 signal amplification /shielding for a cloud below/ above the SO₂ layer. One can see that the
17 error (slope) dramatically increases when the cloud is at a height similar to the SO₂ bulk
18 altitude.

19 *Error source 16 : Cloud correction*

20 Sensitivity tests showed that applying the independent pixel approximation or assuming
21 cloud-free pixels makes a difference of only 5% on yearly averaged data (for anthropogenic
22 BL SO₂ VC with cloud fractions less than 40%).

23 *Error source 17: Cloud model*

24 Cloud As Layer (CAL) is the baseline of the S5P cloud algorithm, but a Lambertian Equivalent
25 Reflector (LER) implementation will be used for NO₂, SO₂ and HCHO retrievals. The error due
26 to the choice of the cloud model will be evaluated during the operational phase.

27 *Error source 18: Profile shape*



1 A major source of systematic uncertainty for most SO₂ scenes is the shape of the vertical SO₂
2 distribution. The corresponding AMF error can be estimated through Eq. 14 and estimation
3 of uncertainty on the profile shape. Note that vertical columns are provided with their
4 averaging kernels, so that column data might be improved for particular locations by using
5 more accurate SO₂ profile shapes based on input from models or observations.

6 For anthropogenic SO₂ under clear-sky conditions, sensitivity tests using a box profile from 0
7 to 1±0.5 km above ground level, or using the different profiles from the CAMELOT study
8 (Levelt et al., 2009), give differences in AMFs in the range of 20-35%. Note that for particular
9 conditions SO₂ may also be uplifted above the top of the boundary layer and sometimes
10 reach upper-tropospheric levels (e.g., Clarisse et al., 2011). SO₂ weighting functions displayed
11 in Figure 5 show that the measurement sensitivity is then increased up to factor of 3 and
12 therefore constitutes a major source of error.

13 In the SO₂ algorithm, the uncertainty on the profile shape is estimated using one parameter
14 describing the shape of the TM5 profile: the profile height, i.e. the altitude (pressure) below
15 which resides 75% of the integrated SO₂ profile. $\frac{\partial M}{\partial s}$ is approached by $\frac{\partial M}{\partial s_h}$ where s_h is half of
16 the profile height. Relatively small variations of this parameter have a strong impact on the
17 total air mass factors for low albedo scenes, because altitude-resolved air mass factors
18 decrease strongly in the lower troposphere, where the SO₂ profiles peak (see e.g. Figure 5).

19 For volcanic SO₂, the effect of the profile shape uncertainty depends on the surface or cloud
20 albedo. For low albedo scenes (Fig 5a), if no external information on the SO₂ plume height is
21 available, it is a major source of error at all wavelengths. Vertical columns may vary up to a
22 factor of 5. For high albedo scenes (Fig 5b), the error is less than 50%. It should be noted that
23 these conditions are often encountered for strong eruptions injecting SO₂ well above the
24 cloud deck (high reflectivity). Further uncertainty on the retrieved SO₂ column may arise if
25 the vertical distribution shows distinct layers at different altitudes, due to the different
26 nature of successive phases of the eruption.

27 In the SO₂ algorithm, three 1km thick box profiles are used in the AMF calculations, mostly to
28 represent typical volcanic SO₂ profiles. The error due to the profile shape uncertainty is
29 estimated by varying the box center levels by 100 hPa.



1 *Error source 19: Aerosols*

2 The effect of aerosols on the air mass factors are not explicitly considered in the SO₂
3 retrieval algorithm. To some extent, however, the effect of the non-absorbing part of the
4 aerosol extinction is implicitly included in the cloud correction (Boersma et al., 2004).
5 Indeed, in the presence of aerosols, the cloud detection algorithm is expected to
6 overestimate the cloud fraction, resulting partly in a compensation effect for cases where
7 aerosols and clouds are at similar heights. Absorbing aerosols have a different effect on the
8 air mass factors, and can lead to significant errors for high aerosol optical depths (AODs). In
9 the TROPOMI SO₂ product, the absorbing aerosol index field can be used to identify
10 observations with elevated absorbing aerosols.

11 Generally speaking, the effect of aerosols on AMF is highly variable and strongly depends on
12 aerosols properties (AOD, height and size distribution, single scattering albedo, scattering
13 phase function, etc.). Typical AMFs uncertainties due to aerosols found in the literature are
14 given in Table 6. As aerosols affect cloud fraction, cloud top height and to some extent the
15 albedo database used, correlations between uncertainties on these parameters are to be
16 expected.

17 *Error source 20: Temperature correction*

18 The DOAS scheme uses an SO₂ cross-section at only one temperature (Bogumil et al., 2003,
19 at 203K) which is in general not representative of the effective temperature corresponding
20 to the SO₂ vertical profile. This effect is in principle accounted for by the temperature
21 correction (which is applied in practice to the AMFs, see section 2.2.3.7) but with a certain
22 error associated of ~5%.

23 **4. VERIFICATION**

24 The SO₂ retrieval algorithm presented in section 2, and hereafter referred as ‘prototype
25 algorithm’, has been applied to OMI and GOME-2 spectra. The results have been extensively
26 verified and validated against different satellite and ground-based data sets (e.g., Theys et
27 al., 2015; Fioletov et al., 2016; Wang et al., 2016). Here we report on further scientific
28 verification activities that took place during the ESA S5P L2WG project.



1 In addition to the prototype algorithm, a scientific algorithm (referred as ‘verification
2 algorithm’) has been developed in parallel. Both algorithms have been applied to synthetic
3 and real (OMI) spectra and results were compared. In this study, we only present and discuss
4 a selection of results (for OMI).

5

6 **4.1 VERIFICATION ALGORITHM**

7 The S5P TROPOMI Verification Algorithm was developed in close cooperation between the
8 *Max Planck Institute for Chemistry* (MPIC) in Mainz (Germany) and the *Institut für Methodik
9 und Fernerkundung* as part of the *Deutsches Institut für Luft- und Raumfahrt
10 Oberpfaffenhofen* (DLR-IMF). Like the prototype algorithm (PA), the verification algorithm
11 (VA) uses a multiple fitting window DOAS approach to avoid non-linear effects during the
12 SCD retrieval in case of high SO₂ concentrations in volcanic plumes. However, especially the
13 alternatively used fitting windows differ strongly from the ones used for the PA and are
14 entirely located in the lower UV range:

- 15 • 312.1-324 nm (*standard retrieval - SR*): Similar to baseline PA fitting window, ideal for
16 small columns
- 17 • 318.6-335.1 nm (*medium retrieval - MR*): This fitting window is essentially located in
18 between the first and second fitting window of the PA and was mainly introduced to
19 guarantee a smoother transition between the baseline window and the one used for
20 high SO₂ concentrations. The differential SO₂ spectral features are still about one
21 order of magnitude smaller than in the baseline window.
- 22 • 323.1-335.1 nm (*alternative retrieval - AR*): Similar to the intermediate fitting window
23 of the PA. This fitting window is used in case of high SO₂ concentrations. Although it
24 is expected that volcanic events with extreme SO₂ absorption are still affected by
25 non-linear absorption in this window, the wavelength range is sufficient for most
26 volcanic events.

27



1 Furthermore, the VA selection criteria for the transition from one window to another are
2 not just based on fixed SO₂ SCD thresholds. The algorithm allows for a slow and smooth
3 transition between different fit ranges by linearly decreasing the weight of the former
4 fitting window and at the same time increasing the weight of the following fitting
5 window:

6 1) for SO₂ SCD ≤ 4x10¹⁷ molec/cm² (≈ 15 DU):

$$SO_2 \text{ SCD} = SR$$

7 2) for 4x10¹⁷ molec/cm² < SO₂ SCD < 9x10¹⁷ molec/cm²:

$$SO_2 \text{ SCD} = SR * \left[1 - \frac{SR}{9 \times 10^{17} \text{ molec/cm}^2} \right] + MR * \left[\frac{SR}{9 \times 10^{17} \text{ molec/cm}^2} \right]$$

8 3) for SO₂ SCD ≥ 9 x 10¹⁷ molec/cm² (≈ 33 DU):

$$SO_2 \text{ SCD} = MR$$

9 4) for 9 x 10¹⁷ molec/cm² < SO₂ SCD < 4.6 x 10¹⁸ molec/cm²:

$$SO_2 \text{ SCD} = MR * \left[1 - \frac{MR}{4.6 \times 10^{18} \text{ molec/cm}^2} \right] + AR * \left[\frac{MR}{4.6 \times 10^{18} \text{ molec/cm}^2} \right]$$

10 5) for SO₂ SCD ≥ 4.6 x 10¹⁸ molec/cm² (≈171 DU):

$$SO_2 \text{ SCD} = AR$$

11 To convert the final SO₂ SCDs into vertical column densities, a single-wavelength AMF for
12 each of the three fitting windows (SO₂ SR, MR and AR) is calculated using the LIDORT LRRS
13 v2.3 (Spurr et al., 2008). The AMF depends on the viewing angles and illumination, surface
14 and cloud conditions as well as on the O₃ total column, which is taken from the O₃ total
15 column retrieval. A cloudy and clear-sky AMF is calculated using temperature dependent

16 cross-sections for SO₂ (Bogumil et al., 2003) and O₃ (Brion et al., 1983): $AMF(\lambda) = \frac{\ln\left(\frac{I+SO_2}{I-SO_2}\right)}{\tau_{SO_2}}$



1 with (I_{+SO_2}) and (I_{-SO_2}) being simulated Earthshine spectra with and without including SO_2 as a
2 trace gas, respectively. Both AMFs are combined using the cloud fraction information. Like
3 the PA, the VA is calculated for different a-priori SO_2 profiles (centre of mass at 2.5 km, 6 km
4 and 15 km) and a temperature correction is applied (see Section 2.2.3.7). In contrast to the
5 PA the VA uses Gaussian-shaped SO_2 profiles with a FWHM of 2.5km rather than box profiles
6 as in the PA. This choice however has only a minor influence on the AMF.

7 For further details on the VA, the reader is referred to the S5P Science Verification Report
8 (available at: https://earth.esa.int/web/sentinel/user-guides/sentinel-5p-tropomi/document-library/-/asset_publisher/w9Mnd6VPjXlc/content/sentinel-5p-tropomi-science-verification-report) for more detailed description and results.

11

12 **4.2 VERIFICATION RESULTS**

13 For the inter-comparison, the prototype algorithm and verification algorithm were applied
14 to OMI data for three different SO_2 emission scenarios: moderate volcanic SO_2 VCDs on May
15 1, 2005, caused by the eruption of the Anatahan volcano, elevated anthropogenic SO_2 VCDs,
16 on May 1, 2005, from the Norilsk copper smelter (Russia), and strongly enhanced SO_2 VCDs,
17 on August 8, 2008, after the massive eruption of Mount Kasatochi.

18 In the following, both algorithms use the same assumption of an SO_2 plume located at 15 km
19 altitude for the AMF calculation. Even if this choice is not realistic for some of the presented
20 scenarios, it minimizes the influence of differences in the a-priori settings. Main deviations
21 between Prototype and Verification Algorithm are therefore expected to be caused by the
22 usage of different fit windows (determining their sensitivity and fit error) and especially the
23 corresponding transition criteria.

24 Figure 9 shows the resulting maps of the SO_2 VCD for the VA (upper panels) and PA (lower
25 panels) for the three selected test cases. As can be seen, both algorithms result in similar SO_2
26 VCDs, however, a closer look reveals some differences, such as the maximum VCDs which
27 are not necessarily appearing at the same locations. For the Anatahan case for instance, the
28 maximum VCD is seen closer to the volcano at the eastern end of the plume for the PA,
29 while it appears to be further downwind for the VA. This effect can be explained by the
30 corresponding fit windows used for both algorithms which may result in deviating SO_2 VCDs,



1 especially for SO₂ scenarios where the best choice is difficult to assess. This is illustrated in
2 Figure 10 showing scatter plots of VA versus PA SO₂ VCDs for the three test cases (Anatahan,
3 Norilsk and Kasatochi) color-coded differently depending on the fitting window used for VA
4 (left) and PA (right), respectively. While the PA uses strictly separated results from the
5 individual fit windows, the VA allows a smooth transition whenever resulting SO₂ SCDs are
6 found to be located in between subsequent fit ranges.

7 For all three test cases, it appears that the PA is less affected by data scattering for low SO₂
8 or SO₂ free measurements than the VA. For the shortest UV fit windows, both algorithms
9 mainly agree but VA VCDs tend to be higher by 10-15% than the PA VCDs for the Anatahan
10 and Kasatochi measurements but interestingly not for the Norilsk case. For SO₂ VCDs around
11 7 DU the PA seem to be slightly affected by saturation effects in 312-326 nm window while
12 VA already makes use of a combined SR/MR SCD. For larger SO₂ VCDs (> 10 DU), data sets
13 from both algorithms show an increased scattering, essentially resulting from the more
14 intensive use of fitting windows at longer wavelengths (for which the SO₂ absorption is
15 weaker). While it is difficult to conclude which algorithm is closer to the actual SO₂ VCDs, the
16 combined fit windows of the VA probably are better suited (in some SO₂ column ranges) for
17 such scenarios as the SO₂ cross-section is generally stronger for lower wavelength (< 325
18 nm) when compared to the intermediate fit window of the PA.

19 For extremely high SO₂ loadings, i.e. for the Kasatochi plume on August 8, 2008, the DOAS
20 retrievals from PA and VA require all three fit windows to prevent systematic
21 underestimation of the resulting SO₂ SCDs due to non-linear absorption caused by very high
22 SO₂ concentrations within the volcanic plume. Figure 9 (right panel) shows that the SO₂
23 distribution is similar for both algorithms, including the location of the maximum SO₂ VCD.

24 From Figure 10 (lowest panel), it can be seen that the VA shows higher values for SO₂ VCDs
25 <100 DU, for all three fit windows. For very high SO₂ VCDs, it seems that the Verification
26 Algorithm is already slightly affected by an underestimation of the SO₂ VCD caused by non-
27 linear radiative transfer effects in the SO₂ AR fit window, while the PA retrievals in the 360-
28 390 nm fit range are insensitive to saturation effects. We note, however, that the Kasatochi
29 plume contained also significant amounts of volcanic ash and we cannot rule out a possible
30 retrieval effect of volcanic ash on the observed differences between PA and VA SO₂ results.
31 Finally we have also investigated other cases with extreme concentrations of SO₂, and



1 contrasting results were found compared to the Kasatochi case. E.g., on September 4, 2014,
2 PA retrieved up to 260 DU of SO₂ during the Icelandic Bardarbunga fissure eruption while VA
3 only found 150 DU (not shown). Compared to Kasatochi, we note that this specific scenario
4 is very different as for the plume height (the SO₂ plume was typically in the lowermost
5 troposphere ~ 3km a.s.l.) and it is likely to play a role in the discrepancy between PA and VA
6 results.

7 In summary, we found that the largest differences between prototype and verification
8 algorithms are due to the fitting window transitions and differences of measurement
9 sensitivity of the fitting windows used (all subject differently to non-linear effects).
10 Verification results have shown that the prototype algorithm produces reasonable results for
11 all the expected scenarios, from modest to extreme SO₂ columns, and are therefore
12 adequate for treating the TROPOMI data. In a future processor update, the method could
13 however be refined.

14

15 **5. VALIDATION OF TROPOMI SO₂ PRODUCT**

16 In this section, we give a brief summary of possibilities (and limitations) to validate the
17 TROPOMI SO₂ product with independent measurements.

18 Generally speaking, the validation of a satellite SO₂ column product is a challenge for several
19 reasons, on top of which is the representativeness of the correlative data when compared to
20 the satellite retrievals. Another reason comes from the wide range of SO₂ columns in the
21 atmosphere that vary from about 1DU level for anthropogenic SO₂ and low level volcanic
22 degassing to 10-1000 DU for medium to extreme volcanic explosive eruptions.

23 The space-borne measurement of anthropogenic SO₂ is difficult because of the low column
24 amount and reduced measurement sensitivity close to the surface. The SO₂ signal is covered
25 by the competing O₃ absorption and the column accuracy is directly affected by the quality
26 of the background correction applied. Among the many parameters of the SO₂ retrieval
27 algorithm that affect the results, the SO₂ vertical profile shape is of utmost importance for
28 any comparison with correlative data. The SO₂ column product accuracy is also directly
29 impacted by the surface albedo used as input for the AMF calculation, the cloud



1 correction/filtering and aerosols. In principle, all these effects will have to be addressed in
2 future validation efforts.

3 The measurement of volcanic SO₂ is facilitated by SO₂ columns often larger than for
4 anthropogenic SO₂. However, the total SO₂ column is strongly dependent on the height of
5 the SO₂ plume which is highly variable and usually unknown. For most volcanoes, there is no
6 ground-based equipment to measure SO₂ during an appreciable eruption and even if it is the
7 case, the data are generally difficult to use for validation. For strong eruptions, volcanic
8 plumes are transported over long-distances and can be measured by ground-based and
9 aircraft devices but generally there is only a handful of datasets available and the number of
10 coincidences is rather small.

11 For both anthropogenic and volcanic SO₂ measurements, the vertical distribution of SO₂ is a
12 key parameter limiting the product accuracy. If reliable (external) information on the SO₂
13 profile (or profile shape) is available, it is recommended to recalculate the SO₂ vertical
14 columns by using this piece of information and the column averaging kernels that can be
15 found in the TROPOMI SO₂ L2 files.

16 **5.1 GROUND-BASED MEASUREMENTS**

17 When considering the application of ground-based instruments for the validation of satellite
18 SO₂ observations, several types of instruments are to be considered.



1 Brewer instruments have the advantage to operate as part of a network
2 (<http://www.woudc.org>), but the retrieved SO₂ columns are generally found inaccurate for
3 the validation of anthropogenic SO₂. Yet in some cases they might be used for coincidences
4 with volcanic clouds, typically for SO₂ VCDs larger than 5-10 DU.
5 Multi-axis DOAS (MAX-DOAS) or direct-sun DOAS measurements (e.g., from Pandora
6 instruments) can be used to validate satellite SO₂ columns from anthropogenic emissions
7 (e.g., Theys et al., 2015; Jin et al., 2016; Wang et al., 2016), but cautiousness must be exerted
8 in the interpretation of the results because realistic SO₂ profile shapes must be used by the
9 satellite retrieval scheme. While direct-sun DOAS retrievals are independent of the SO₂
10 profile shape, MAX-DOAS observations carry information on the SO₂ vertical distribution but
11 it is not obvious that the technique is directly applicable to the validation of satellite SO₂
12 retrievals, because the technique is not able to retrieve the full SO₂ profile. Another
13 important limitation comes from the fact that ground-based DOAS and satellite instruments
14 have very different fields of view and are therefore probing different air masses. This can
15 cause large discrepancy between ground-based and satellite measurements in case of strong
16 horizontal gradients of the SO₂ column field.
17 DOAS instruments scanning through volcanic plumes are now routinely measuring volcanic
18 SO₂ emissions, as part of the Network for Observation of Volcanic and Atmospheric Change
19 (NOVAC; Galle et al., 2010), for an increasing number of degassing volcanoes. Ongoing
20 research focusses on calculating SO₂ fluxes from those measurements and accounting for
21 non-trivial radiative transfer effects (e.g. light dilution, see Kern et al., 2009). NOVAC flux
22 data could be used for comparison with TROPOMI SO₂ data but it requires techniques to
23 convert satellite SO₂ vertical column into mass fluxes (see e.g., Theys et al., 2013, and
24 references therein, Beirle et al., 2014). Similarly, fast-sampling UV cameras are becoming
25 increasingly used to measure and invert SO₂ fluxes and are also relevant to validate
26 TROPOMI SO₂ data over volcanoes or anthropogenic point sources (e.g., power plants). It
27 should be noted, however, that ground-based remote-sensing instruments operating nearby
28 SO₂ point sources are sensitive to newly emitted SO₂ plumes while a satellite sensor like
29 TROPOMI will measure aged plumes that have been significantly depleted in SO₂. While in
30 some cases it is possible to compensate for this effect by estimating the SO₂ lifetime e.g.
31 directly from the space measurements (Beirle et al., 2014), the general situation is that the



1 SO₂ loss rate is highly variable (especially in volcanic environments) and this can lead to
2 strong discrepancies when comparing satellite and ground-based SO₂ fluxes.

3 In addition to optical devices, there are also in-situ instruments measuring surface SO₂
4 mixing ratios. This type of instrument can only validate surface concentrations, and
5 additional information on the SO₂ vertical profile (e.g., from model data) is required to make
6 the link with the satellite retrieved column. However, in-situ instruments are being operated
7 for pollution monitoring in populated areas, and allow for extended and long term
8 comparisons with satellite data (see e.g. Nowlan et al., 2011).

9 **5.2 AIRCRAFT AND MOBILE MEASUREMENTS**

10 Airborne and mobile instruments provide valuable and complementary data for satellite
11 validation.

12 In case of volcanic explosive eruptions, satisfactory validation results can be obtained by
13 comparing satellite and fixed ground DOAS measurements of drifting SO₂ plumes, as shown
14 by Spinei et al. (2008), but the comparison generally suffers from the small number of
15 coincidences. Dedicated aircraft campaign flights (e.g. Schumann et al., 2011) can in
16 principle improve the situation. Their trajectory can be planned with relative ease to cross
17 sustained eruptive plumes. However, localized high SO₂ concentrations, may be carried away
18 too quickly to be captured by aircraft or have diluted below the threshold limit for satellite
19 detection before an aircraft can respond. An important data base of SO₂ aircraft
20 measurements is provided by the CARIBIC/IAGOS project which exploits automated scientific
21 instruments operating long distance commercial flights. Measurements of volcanic SO₂
22 during the eruptions of Mt. Kasatochi and Eyjafjallajökull and comparison with satellite data
23 have been reported by Heue et al. (2010, 2011).



1 An attempt to validate satellite SO₂ measurements using mobile DOAS instrument for a fast
2 moving (stratospheric) volcanic SO₂ plume was presented by Carn and Lopez (2011).
3 Although the agreement between both data sets was found reasonable, the comparison was
4 complicated by the relatively fast displacement of the volcanic cloud with respect to the
5 ground spectrometer and clear heterogeneity on scales smaller than a satellite pixel. For
6 degassing volcanoes or newly fissure eruptions, mobile DOAS traverse measurements under
7 the plume offer unique opportunities to derive volcanic SO₂ fluxes that could be used to
8 validate satellite measurements.

9 For polluted regions, measurements of anthropogenic SO₂ by airborne nadir-looking DOAS
10 sensors are able to produce high spatial resolution mapping of the SO₂ column field (e.g.,
11 during the AROMAT campaigns, <http://uv-vis.aeronomie.be/aromat/>) that could be used to
12 validate TROPOMI SO₂ product or give information on horizontal gradients of the SO₂ field
13 (e.g. in combination with coincident mobile DOAS measurements) that would be particularly
14 useful when comparing satellite and MAX-DOAS data (see discussion in section 5.1). Equally
15 important are also limb-DOAS or in-situ instruments to provide information on vertical
16 distribution of SO₂ which is crucial for satellite validation (e.g., Krotkov et al., 2008).

17 **5.3 SATELLITE MEASUREMENTS**

18 Inter-comparison of satellite SO₂ measurements generally provides a convenient and easy
19 way to evaluate at a glance the quality of a satellite product, by comparing SO₂ maps for
20 instance. Often, it also provides improved statistics and geographical representativeness but
21 it poses a number of problems because when different satellite sensors are compared they
22 have also different overpass times, swaths, spatial resolutions and measurement sensitivities
23 to SO₂.

24



1 For volcanic SO₂, satellite measurements often provide the only data available for the first
2 hours to days after an eruption event and satellite inter-comparison is thus the only practical
3 way to assess the quality of the retrievals. To overcome sampling issues mentioned above,
4 inter-comparison of SO₂ masses integrated over the measured volcanic plume is often
5 performed. For TROPOMI, current satellite instruments will be an important source of data
6 for cross-comparisons. Although non-exhaustive, the list of satellite sensors that could be
7 used is: OMI, OMPS, GOME-2 and IASI (MetOp-A, -B, and the forthcoming -C), AIRS, CrIS,
8 VIIRS and MODIS. As mentioned above, the inter-comparison of satellite SO₂ products is
9 difficult and in this respect the plume altitude is a key-factor of the satellite SO₂ data
10 accuracy. Comparison of TROPOMI and other satellite SO₂ products will benefit from the
11 advent of scientific algorithms for the retrieval of SO₂ plume heights but also from the use of
12 volcanic plume height observations using space lidar instruments (e.g. CALIOP and the future
13 EarthCare mission).

14 For both anthropogenic SO₂ and volcanic degassing SO₂, the satellite UV sensors OMI, GOME-
15 2 and OMPS can be compared to TROPOMI SO₂ data by averaging data over certain polluted
16 regions. It will give valuable information on the data quality but, in some cases, the
17 comparison will suffer from differences in spatial resolution. A more robust and in-depth
18 comparison would be to use different TROPOMI SO₂ datasets generated by different
19 retrieval algorithms and investigate the differences in the various retrieval steps (spectral
20 fitting, corrections, radiative transfer simulations, error analysis).

21

22 **6 CONCLUSIONS**

23 Based on the heritage from GOME, SCIAMACHY, GOME-2 and OMI, a DOAS retrieval
24 algorithm has been developed for the operational retrieval of SO₂ vertical columns from
25 TROPOMI Level1b measurements in the UV spectral range. Here we describe its main
26 features.

27 In addition to the traditionally used fitting window of 312-326 nm, the new algorithm allows
28 for the selection of two additional fitting windows (325-335 nm and 360-390nm), reducing
29 the risk of saturation and ensuring accurate SO₂ column retrieval even for extreme SO₂



1 concentrations as observed for major volcanic events. The spectral fitting procedure also
2 includes an advanced wavelength calibration scheme and a spectral spike removal algorithm.

3 After the slant column retrieval, the next step is a background correction, which is
4 empirically based on the O₃ slant column (for the baseline fitting window) and across-track
5 position, and accounts for possible across-track dependencies and instrumental degradation.

6 The SO₂ slant columns are then converted into vertical columns by the means of air mass
7 factor calculations. The latter is based on weighting function look-up-tables with
8 dependencies on the viewing geometry, clouds, surface pressure, albedo, ozone, and is
9 applied to pre-defined box profiles and TM5 CTM forecast profiles. In addition, the algorithm
10 computes DOAS-type averaging kernels and a full error analysis of the retrieved columns.

11 In this paper we have also presented verification results using an independent algorithm for
12 selected OMI scenes with enhanced SO₂ columns. Overall the prototype algorithm agrees
13 well with the verification algorithm, demonstrating its ability in retrieving accurately medium
14 to very high SO₂ columns. We have discussed the advantages and limitations of both
15 prototype and verification algorithms.

16 Based on the experience with GOME-2 and OMI, the TROPOMI SO₂ algorithm is expected to
17 have a comparable level of accuracy. Due to its high signal-to-noise ratio, TROPOMI will be
18 capable of at least achieving comparable retrieval precision as its predecessors but at a
19 much finer spatial resolution of 7x3.5 km² at best. For single measurements, the user
20 requirements for tropospheric SO₂ concentrations will not be met, but improved monitoring
21 of strong pollution and volcanic events will be possible by spatial and temporal averaging the
22 increased number of observations of TROPOMI. Nevertheless, it will require significant
23 validation work and here we have discussed some of the inherent challenges for both
24 volcanic and anthropogenic SO₂ retrievals. Correlative measurements from ground-based,
25 aircraft/mobile, and satellite instruments, will be needed over different regions and various
26 emission scenarios to assess and characterize the quality of TROPOMI SO₂ retrievals.



1 The baseline algorithm presented here, including all its modules (slant column retrieval,
2 background correction, air mass factor calculation and error analysis), has been fully
3 implemented in the S5P operational processor UPAS by the DLR team. Figure 11 illustrates
4 the status of the implementation for one day of OMI test data, exemplarily for the slant
5 columns retrievals. A nearly perfect agreement is found between SCD results over 4 orders
6 of magnitude. A similar match between prototype algorithm and operational processor is
7 found for all other retrieval modules.

8 For more information on the TROPOMI SO₂ L2 data files, the reader is referred to the S5P
9 SO₂ Product User Manual (Pedergrana et al., 2016).

10 **APPENDIX A. FEASIBILITY, INFORMATION ON DATA PRODUCT AND ANCILLARY DATA**

11 **High level data product description**

12 In addition to the main product results, such as SO₂ slant column, vertical column and air
13 mass factor, the level 2 data files will contain several additional parameters and diagnostic
14 information. Table A1 gives a minimum set of data fields that will be present in the Level 2
15 data. A 1-orbit SO₂ column Level 2 file will be of about 640 MB. More details about the
16 operational level 2 product based on the netCDF data format and the CF metadata
17 convention are provided in the SO₂ Product User Model (Pedergrana et al., 2016).

18 It should be noted that the averaging kernels are given only for the a-priori profiles from the
19 TM5 CTM (to save space). The averaging kernels for the box profiles can be estimated by
20 scaling the provided averaging kernel (corresponding to TM5 profiles): $AK_{\text{box}}(p)$
21 $=AK(p) \cdot \text{Scaling box}$. Following the AK formulation of Eskes and Boersma (2004), the scaling
22 factor is given simply by AMFs ratios: $AMF_{\text{TM5}}/AMF_{\text{box}}$.

23 **Auxiliary information**

24 The algorithm relies on several external data sets. These can be either static or dynamic. An
25 overview is given in Table A2 and A3.

26 **ACKNOWLEDGEMENTS**

27 This work has been performed in the frame of the TROPOMI project. We acknowledge
28 financial support from ESA S5P, Belgium Prodex TRACE-S5P projects, and Bayerisches



1 Staatsministerium für Wirtschaft und Medien, Energie und Technologie (grant 07 03/893 73/
2 5 /2013).

3

4 REFERENCES

5 Afe, O. T., Richter, A., Sierk, B., Wittrock, F., and Burrows, J.P.: BrO emissions from
6 volcanoes: a survey using GOME and SCIAMACHY measurements, *Geophys. Res. Lett.*, 31,
7 L24113, 2004.

8

9 Beirle, S., Hörmann, C., Penning de Vries, M., Dörner, S., Kern, C., and Wagner, T.: Estimating
10 the volcanic emission rate and atmospheric lifetime of SO₂ from space: a case study for
11 Kīlauea volcano, Hawai, *Atmos. Chem. Phys.*, 14, 8309-8322, doi:10.5194/acp-14-8309-2014,
12 2014.

13

14 Bobrowski, N., Kern, C., Platt, U., Hörmann, C., and Wagner, T.: Novel SO₂ spectral
15 evaluation scheme using the 360–390 nm wavelength range, *Atmos. Meas. Tech.*, 3, 879-
16 891, doi:10.5194/amt-3-879-2010, 2010.

17

18 Boersma, K. F., Eskes, H. J., and Brinksma, E. J.: Error analysis for tropospheric NO₂ retrieval
19 from space, *J. Geophys. Res.*, 109, D04311, doi: 10.1029/2003JD003962, 2004.

20

21 Bogumil, K., Orphal, J., Homann, T., Voigt, S., Spietz, P., Fleischmann, O., Vogel, A.,
22 Hartmann, M., Bovensmann, H., Frerick, J., and Burrows, J.P.: Measurements of molecular
23 absorption spectra with the SCIAMACHY Pre-Flight Model: instrument characterization and
24 reference data for atmospheric remote-sensing in the 230-2380 nm region, *Journal of*
25 *Photochemistry and Photobiology A*, 157, 167-184, 2003.

26



1 Bovensmann, H., Peuch, V.-H., van Weele, M., Erbertseder, T., and Veihelmann, B.: Report Of
2 The Review Of User Requirements For Sentinels-4/-5, ESA, EOP-SM/2281/BV-bv, issue: 2.1,
3 2011.

4

5 Brenot, H., Theys, N., Clarisse, L., van Geffen, J., van Gent, J., Van Roozendael, M.,
6 van der A, R., Hurtmans, D., Coheur, P.-F., Clerbaux, C., Valks, P., Hedelt, P., Prata, F.,
7 Rasson, O., Sievers, K., and Zehner, C.: Support to Aviation Control Service (SACS): an online
8 service for near real-time satellite monitoring of volcanic plumes, Nat. Hazards Earth Syst.
9 Sci., 14, 1099-1123, doi:10.5194/nhess-14-1099-2014, 2014.

10

11 Brion, J., Chakir, A., Charbonnier, J., et al.: Absorption spectra measurements for the ozone
12 molecule in the 350-830 nm region, J. Atmos. Chem., 30, 291-299,
13 doi:10.1023/A:1006036924364, 1998.

14

15 Carn, S.A., and Lopez, T.M.: Opportunistic validation of sulfur dioxide in the Sarychev peak
16 volcanic eruption cloud, Atmos. Meas. Tech., 4, 1705-1712, 2011.

17 Carn, S.A., Clarisse, L., and Prata, A.J.: Multi-decadal satellite measurements of global
18 volcanic degassing, J. Volcanol. Geotherm. Res., 311, 99-134,
19 <http://dx.doi.org/10.1016/j.jvolgeores.2016.01.002>, 2016.

20

21 Chance, K., and Spurr, R. J.: Ring effect studies: Rayleigh scattering including molecular
22 parameters for rotational Raman scattering, and the Fraunhofer spectrum, Applied Optics,
23 36, 5224-5230, 1997.

24

25 Chance, K., and Kurucz, R. L.: An improved high-resolution solar reference spectrum for
26 earth's atmosphere measurements in the ultraviolet, visible, and near infrared, J. Quant.
27 Spectrosc. Radiat. Transf., 111(9), 1289-1295, 2010.



1

2 Clarisse, L., Fromm, M., Ngadi, Y., Emmons, L., Clerbaux, C., Hurtmans, D., and Coheur, P.-F.:
3 Intercontinental transport of anthropogenic sulfur dioxide and other pollutants; an infrared
4 remote sensing case study, *Geophys. Res. Lett.*, 38, L19806, doi:10.1029/2011GL048976,
5 2011.

6

7 Danielson, J.J., and Gesch, D.B.: Global multi-resolution terrain elevation data 2010
8 (GMTED2010): U.S. Geological Survey Open-File Report 2011–1073, 26 p, 2011.

9

10 De Smedt, I., Müller, J.-F., Stavrou, T., van der A, R., Eskes, H., and Van Roozendaal, M.:
11 Twelve years of global observation of formaldehyde in the troposphere using GOME and
12 SCIAMACHY sensors, *Atmos. Chem. Phys.*, 8, 4947-4963, 2008.

13

14 De Smedt, I., et al.: Formaldehyde retrievals from TROPOMI onboard Sentinel-5 Precursor:
15 Algorithm Theoretical Basis, in preparation for *Atmos. Meas. Tech.*, 2016.

16

17 Eisinger, M., and Burrows, J.P.: Tropospheric sulfur dioxide observed by the ERS-2 GOME
18 instrument, *Geophys. Res. Lett.*, Vol. 25, pp. 4177-4180, 1998.

19

20 Eskes, H. J., and Boersma, K. F.: Averaging kernels for DOAS total column satellite retrievals,
21 *Atmos. Chem. Phys.*, 3, 1285–1291, 2003.

22

23 Fioletov, V. E., McLinden, C. A., Krotkov, N., Yang, K., Loyola, D. G., Valks, P.,
24 They, N., Van Roozendaal, M., Nowlan, C. R., Chance, K., Liu, X., Lee, C.,
25 and Martin, R. V.: Application of OMI, SCIAMACHY, and GOME-2 satellite SO₂ retrievals for



1 detection of large emission sources, *J. Geophys. Res. Atmos.*, **118**, 11,399–11,418,
2 doi:10.1002/jgrd.50826, 2013.

3

4 Fioletov, V.E., McLinden, C.A., Krotkov, N.A., Li, C., Joiner, J., Theys, N., Carn, S.A., and
5 Moran, M.D.: A global catalogue of large SO₂ sources and emissions derived from the Ozone
6 Monitoring Instrument, *Atmos. Chem. Phys. Discuss.*, doi:10.5194/acp-2016-417, 2016.

7

8 Galle, B., Johansson, M., Rivera, C., Zhang, Y., Kihlman, M., Kern, C., Lehmann, T., Platt, U.,
9 Arellano, S., and Hidalgo, S.: Network for Observation of Volcanic and Atmospheric Change
10 (NOVAC) – A global network for volcanic gas monitoring: Network layout and instrument
11 description, *J. Geophys. Res.*, **115**, D05304, doi:10.1029/2009JD011823, 2010.

12

13 Heue K.-P., Brenninkmeijer, C.A.M., Wagner, T., Mies, K., Dix, B., Frieß, U., Martinsson, B. G.,
14 Šlemr, F., and van Velthoven, P.F.J.: Observations of the 2008 Kasatochi volcanic SO₂ plume
15 by CARIBIC aircraft DOAS and the GOME-2 satellite. *Atmos. Chem. Phys.*, **10**, 4699–4713,
16 doi:10.5194/acp-10-4699-2010, 2010.

17

18 Heue, K., Brenninkmeijer, C. A. M., Baker, A. K., Rauthe-Schöch, A., Walter, D., Wagner, T.,
19 Hörmann, C., Sihler, H., Dix, B., Frieß, U., Platt, U., Martinsson, B. G., van Velthoven, P. F. J.,
20 Zahn, A., and Ebinghaus, R.: SO₂ and BrO observation in the plume of the Eyjafjallajökull
21 volcano 2010: CARIBIC and GOME-2 retrievals, *Atmos. Chem. Phys.*, **11**, 2973–2989,
22 doi:10.5194/acp-11-2973-2011, 2011.

23

24 Hendrick, F., Van Roozendaal, M., Kylling, A., Petritoli, A., Rozanov, A., Sanghavi, S.,
25 Schofield, R., von Friedeburg, C., Wagner, T., Wittrock, F., Fonteyn, D., and De Mazière, M.:
26 Intercomparison exercise between different radiative transfer models used for the



- 1 interpretation of ground-based zenith-sky and multi-axis DOAS observations, Atmos. Chem.
2 Phys., 6, 93-108, 2006.
- 3
- 4 Hermans, C., Vandaele, A.C., and Fally, S.: Fourier transform measurements of SO₂
5 absorption cross sections: I. Temperature dependence in the 24 000–29 000 cm⁻¹ (345–420
6 nm) region, J. Quant Spectrosc. Radiat. Transfer, 110, 756–765, doi:
7 10.1016/j.jqsrt.2009.10.031, 2009.
- 8
- 9 Hörmann, C., Sihler, H., Bobrowski, N., Beirle, S., Penning de Vries, M., Platt, U., and Wagner,
10 T.: Systematic investigation of bromine monoxide in volcanic plumes from space by using the
11 GOME-2 instrument, Atmos. Chem. Phys., 13, 4749-4781, doi:10.5194/acp-13-4749-2013,
12 2013
- 13
- 14 Huijnen, V., Williams, J., van Weele, M., van Noije, T., Krol, M., Dentener, F., Segers, A.,
15 Houweling, S., Peters, W., de Laat, J., Boersma, F., Bergamaschi, P., van Velthoven, P., Le
16 Sager, P., Eskes, H., Alkemade, F., Scheele, R., Nédélec, P., and Pätz, H.-W. : The global
17 chemistry transport model tm5: description and evaluation of the tropospheric chemistry
18 version 3.0., Geoscientific Model Development, 3(2):445-473, 2010.
- 19
- 20 Jin, J., Ma, J., Lin, W., Zhao, H., Shaiganfar, R., Beirle, S., and Wagner, T.: MAX-DOAS
21 measurements and satellite validation of tropospheric NO₂ and SO₂ vertical column
22 densities at a rural site of North China, Atmospheric Environment, 133, 12–25, 2016.
- 23
- 24 Kelder, H., van Weele, M., Goede, A., Kerridge, B., Reburn, J., Bovensmann, H., Monks, P.,
25 Remedios, J., Mager, R., Sassier, H., and Baillon, Y.: Operational Atmospheric Chemistry
26 Monitoring Missions – CAPACITY: Composition of the Atmosphere: Progress to Applications
27 in the user Community, Final Report of ESA contract no. 17237/03/NL/GS, 2005.



1 Kern, C., Deutschmann, T., Vogel, A., Wöhrbach, M., Wagner, T., and Platt, U.: Radiative
2 transfer corrections for accurate spectroscopic measurements of volcanic gas emissions,
3 Bull. Volcanol., 72,233-247, 2009.

4

5 Khokhar, M. F., Frankenberg, C., Van Roozendaal, M., Beirle, S., Kühl, S., Richter, A., Platt, U.,
6 and Wagner, T.: Satellite Observations of Atmospheric SO₂ from Volcanic Eruptions during
7 the Time Period of 1996 to 2002, J. Adv. Space Res., 36(5), 879-887,
8 10.1016/j.asr.2005.04.114, 2005.

9

10 Kleipool, Q. L., Dobber, M. R., de Haan, J. F. and Levelt, P. F.: Earth surface reflectance
11 climatology from 3 years of OMI data, J. Geophys. Res., 113(D18), D18308,
12 doi:10.1029/2008JD010290, 2008.

13

14 Koelemeijer, R. B. A., Stammes, P., Hovenier, J. W. and de Haan, J. F.: A fast method for
15 retrieval of cloud parameters using oxygen A band measurements from the Global Ozone
16 Monitoring Experiment, J. Geophys. Res., 106(D4), 3475-3490, doi:10.1029/2000JD900657
17 2001.

18

19 Koelemeijer, R.B.A., de Haan, J.F. and Stammes, P.: A database of spectral surface
20 reflectivity in the range 335-772 nm derived from 5.5 years of GOME observations, J.
21 Geophys. Res., 108(D2), 4070, doi: 10.1029/2002JD002429, 2003.

22

23 Krotkov, N. A., Carn, S. A., Krueger, A. J., Bhartia, P. K., Yang, K.: Band residual difference
24 algorithm for retrieval of SO₂ from the Aura Ozone Monitoring Instrument (OMI), IEEE Trans.
25 Geosci. Remote Sensing, AURA Special Issue, 44(5), 1259-1266,
26 doi:10.1109/TGRS.2005.861932, 2006.

27



1 Krotkov, N. A., et al., Validation of SO₂ retrievals from the Ozone Monitoring Instrument over
2 NE China, *J. Geophys. Res.*, 113, D16S40, doi:10.1029/2007JD008818, 2008.

3

4 Krotkov, N. A., McLinden, C. A., Li, C., Lamsal, L. N., Celarier, E. A., Marchenko, S. V., Swartz,
5 W. H., Bucsela, E. J., Joiner, J., Duncan, B. N., Boersma, K. F., Veefkind, J. P., Levelt, P. F.,
6 Fioletov, V. E., Dickerson, R. R., He, H., Lu, Z., and Streets, D. G.: Aura OMI observations of
7 regional SO₂ and NO₂ pollution changes from 2005 to 2014, *Atmos. Chem. and Phys.*, 16(7),
8 4605-4629, doi:10.5194/acp-15-4605-2016, 2016.

9

10 Krueger A.J.: Sighting of El Chichon sulfur dioxide clouds with the Nimbus 7 total ozone
11 mapping spectrometer, *Science*, 220, 1377–1379, 1983.

12

13 Li, C., Joiner, J., Krotkov, N. A., and Bhartia, P. K.: A fast and sensitive new satellite SO₂
14 retrieval algorithm based on principal component analysis: Application to the ozone
15 monitoring instrument, *Geophys. Res. Lett.*, 40, 6314–6318, doi:10.1002/2013GL058134,
16 2013.

17

18 Langen, J., Meijer, Y., Brinksma, E., Veihelmann, B., and Ingmann, P.: GMES Sentinels 4 and 5
19 Mission Requirements Document (MRD), ESA, EO-SMA-/1507/JL, issue: 3, 2011.

20

21 Lee, C., Martin, R. V., van Donkelaar, A., O’Byrne, G., Krotkov, N., Richter, A., Huey, L. G., and
22 Holloway, J.S.: Retrieval of vertical columns of sulfur dioxide from SCIAMACHY and OMI: Air
23 mass factor algorithm development, validation, and error analysis, *J. Geophys. Res.*, 114,
24 D22303, doi:10.1029/2009JD012123, 2009.

25



1 Levelt, P., Veefkind, J., Kerridge, B., Siddans, R., de Leeuw, G., Remedios, J., and Coheur, P.:
2 Observation Techniques and Mission Concepts for Atmospheric Chemistry (CAMELOT),
3 Report, European Space Agency, Noordwijk, The Netherlands, 2009.

4

5 Loyola et al., S5P Cloud Products ATBD, available at:
6 <https://sentinel.esa.int/web/sentinel/technical-guides/sentinel-5p/appendices/references>
7 and <http://www.tropomi.eu/documents/level-2-products>, 2016.

8

9 Martin, R. V., Chance, K., Jacob, D. J., Kurosu, T. P., Spurr, R. J. D., Bucsela, E., Gleason, J.F.,
10 Palmer, P.I., Bey, I., Fiore, A.M., Li, Q., Yantosca, R.M., and Koelemeijer, R.B.A.: An improved
11 retrieval of tropospheric nitrogen dioxide from GOME, *J. Geophys. Res.*, 107(D20), 4437,
12 doi:10.1029/2001JD001027, 2002.

13

14 McLinden, C.A., Fioletov, V., Shephard, M.W., Krotkov, N., Li, C., Martin, R.V., Moran, M.D.,
15 and Joiner, J.: Space-based detection of missing sulfur dioxide sources of global air pollution,
16 *Nature Geoscience*, 9, 496-500, doi:10.1038/ngeo2724, 2016.

17

18 Nowlan, C.R., Liu, X., Chance, K., Cai, Z., Kurosu, T.P., Lee, C., and Martin, R.V.: Retrievals of
19 sulfur dioxide from the Global Ozone Monitoring Experiment 2 (GOME-2) using an optimal
20 estimation approach: Algorithm and initial validation, *J. Geophys. Res.*, 116, D18301,
21 doi:10.1029/2011JD015808, 2011.

22

23 Palmer, P. I., Jacob, D. J., Chance, K. V., Martin, R. V., D, R. J., Kurosu, T. P., Bey, I., Yantosca,
24 R. and Fiore,A.: Air mass factor formulation for spectroscopic measurements from satellites:
25 Application to formaldehyde retrievals from the Global Ozone Monitoring Experiment,
26 *Journal of Geophysical Research*, 106(D13), 14539-14550, doi:10.1029/2000JD900772, 2001.

27



- 1 Platt, U., and Stutz, J.: Differential Optical Absorption Spectroscopy (DOAS), Principle and
2 Applications, ISBN 3-340-21193-4, Springer Verlag, Heidelberg, 2008.
- 3
- 4 Pedernana, M., et al., S5P Level 2 Product User Manual Sulfur Dioxide SO₂, available at:
5 <https://sentinel.esa.int/web/sentinel/technical-guides/sentinel-5p/appendices/references>
6 and <http://www.tropomi.eu/documents/level-2-products>, 2016.
- 7
- 8 Puķīte, J., Kühn, S., Deutschmann, T., Platt, U., and Wagner, T.: Extending differential optical
9 absorption spectroscopy for limb measurements in the UV, Atmos. Meas. Tech., 3, 631-653,
10 2010.
- 11
- 12 Richter, A., Wittrock, F., Schönhardt, A., and Burrows, J.P.: Quantifying volcanic SO₂
13 emissions using GOME2 measurements, Geophys. Res. Abstr., EGU2009-7679, EGU General
14 Assembly 2009, Vienna, Austria, 2009.
- 15
- 16 Richter, A., Begoin, M., Hilboll, A., and Burrows, J. P.: An improved NO₂ retrieval for the
17 GOME-2 satellite instrument, Atmos. Meas. Tech., 4(6), 213-246, doi:10.5194/amt-4-1147-
18 2011, 2011.
- 19
- 20 Rix, M., Valks, P., Hao, N., Loyola, D. G., Schlager, H., Huntrieser, H. H., Flemming, J., Koehler,
21 U., Schumann, U., and Inness, A.: Volcanic SO₂, BrO and plume height estimations using
22 GOME-2 satellite measurements during the eruption of Eyjafjallajökull in May 2010, J.
23 Geophys. Res., 117, D00U19, doi:10.1029/2011JD016718, 2012.
- 24
- 25 Robock, A.: Volcanic eruptions and climate, Rev. Geophys., 38, 191–219, 2000.
- 26



1 Rozanov, A., Rozanov, V., and Burrows, J. P.: A numerical radiative transfer model for a
2 spherical planetary atmosphere: Combined differential integral approach involving the
3 Piccard iterative approximation, *J. Quant. Spectrosc. Radiat. Transfer*, 69, 491–512, 2001.

4

5 Sanders, B., et al., S5P ATBD of the Aerosol Layer Height product, available at:
6 <https://sentinel.esa.int/web/sentinel/technical-guides/sentinel-5p/appendices/references>
7 and <http://www.tropomi.eu/documents/level-2-products>, 2016.

8

9 Schumann, U., Weinzierl, B., Reitebuch, O., Schlager, H., Minikin, A., Forster, C., Baumann, R.,
10 Sailer, T., Graf, K., Mannstein, H., Voigt, C., Rahm, S., Simmet, R., Scheibe, M., Lichtenstern,
11 M., Stock, P., Růba, H., Schauble, D., Tafferner, A., Rautenhaus, M., Gerz, T., Ziereis, H.,
12 Krautstrunk, M., Mallaun, C., Gayet, J.-F., Lieke, K., Kandler, K., Ebert, M., Weinbruch, S.,
13 Stohl, A., Gasteiger, J., Groß, S., Freudenthaler, V., Wiegner, M., Ansmann, A., Tesche, M.,
14 Olafsson, H., and Sturm, K.: Airborne observations of the Eyjafjalla volcano ash cloud over
15 Europe during air space closure in April and May 2010, *Atmos. Chem. Phys.*, 11, 2245–2279,
16 doi:10.5194/acp-11-2245-2011, 2011.

17

18 Spinei, E., Carn, S.A., Krotkov, N.A., Mount, G.H., Yang, K., and Krueger, A.J.: Validation of
19 ozone monitoring instrument SO₂ measurements in the Okmok volcanic plume over Pullman,
20 WA in July 2008, *J. Geophys. Res.*, Okmok-Kasatochi Special Issue, 115, D00L08,
21 doi:10.1029/2009JD013492, 2010

22

23 Spurr, R., LIDORT and VLIDORT: Linearized pseudo-spherical scalar and vector discrete
24 ordinate radiative transfer models for use in remote sensing retrieval problems. *Light*
25 *Scattering Reviews*, Volume 3, ed. A. Kokhanovsky, Springer, 2008.

26



1 Spurr, R., de Haan, J.F., van Oss, R., and Vasilkov, A.: Discrete Ordinate Radiative Transfer in a
2 Stratified Medium with First Order Rotational Raman Scattering, *J. Quant. Spectros. Rad.*
3 *Transf.*, 2008, 109, 3, 404-425, doi:10.1016/j.jqsrt.2007.08.011, 2008.

4

5 Theys, N., Campion, R., Clarisse, L., Brenot, H., van Gent, J., Dils, B., Corradini, S., Merucci, L.,
6 Coheur, P.-F., Van Roozendael, M., Hurtmans, D., Clerbaux, C., Tait, S., Ferrucci, F.: Volcanic
7 SO₂ fluxes derived from satellite data: a survey using OMI, GOME-2, IASI and MODIS, *Atmos.*
8 *Chem. Phys.*, 13, 5945–5968, 2013.

9

10 Theys, N., De Smedt, I., van Gent, J., Danckaert, T., Wang, T., Hendrick, F., Stavrakou, T.,
11 Bauduin, S., Clarisse, L., Li, C., Krotkov, N. A., Yu, H., Van Roozendael, M.: Sulfur dioxide
12 vertical column DOAS retrievals from the Ozone Monitoring Instrument: Global observations
13 and comparison to ground-based and satellite data, *J. Geophys. Res. Atmos.*, 120,
14 doi:10.1002/2014JD022657, 2015.

15 Thomas, W., Erbertseder, T., Ruppert, T., van Roozendael, M., Verdebout, J., Balis, D., Meleti,
16 C., and Zerefos, C.: On the retrieval of volcanic sulfur dioxide emissions from GOME
17 backscatter measurements, *J. Atmos. Chem.*, 50, 295–320, doi:10.1007/s10874-005-5544-1,
18 2005.

19

20 van der A, R., Mijling, B., Ding, J., Koukouli, M., Liu, F., Li, Q., Mao, H., and Theys, N.: Cleaning
21 up the air: Effectiveness of air quality policy for SO₂ and NO_x emissions in China, *Atmos.*
22 *Chem. Phys. Discuss.*, doi:10.5194/acp-2016-445, in review, 2016.

23

24 Vandaele, A.C., Hermans, C., Simon, P.C., Carleer, M., Colin, R., Fally, S., Mérienne, M.F.,
25 Jenouvrier, A., and Coquart, B.: Measurements of the NO₂ absorption cross-section from
26 42000 cm⁻¹ to 10000 cm⁻¹ (238-1000 nm) at 220 K and 294 K, *J. Quant. Spectrosc. Radiat.*
27 *Transfer*, 59, 171-184, 1998.



1

2 Vandaele, A. C., Hermans, C., and Fally, S.: Fourier transform measurements of SO₂
3 absorption cross sections: II. Temperature dependence in the 29000–44000 cm⁻¹ (227–345
4 nm) region, *J. Quant. Spectrosc. Radiat. Transfer*, 110, 2115–2126,
5 doi:10.1016/j.jqsrt.2009.05.006, 2009.

6

7 van Geffen, J., van Roozendaal, M., Rix, M., and Valks, P.: Initial Validation of GOME-2 GDP
8 4.2 SO₂ Total Columns—ORR B, TN-IASB-GOME2-O3MSAF-SO2-01, Sep. 2008

9

10 van Geffen, J., et al.: S5P NO₂ data products ATBD, available at:
11 <https://sentinel.esa.int/web/sentinel/technical-guides/sentinel-5p/appendices/references>
12 and <http://www.tropomi.eu/documents/level-2-products>, 2016.

13

14 van Weele, M., Levelt, P., Aben, I., Veefkind, P., Dobber, M., Eskes, H., Houweling, S.,
15 Landgraf, J., Noordhoek, R.: Science Requirements Document for TROPOMI. Volume 1,
16 KNMI & SRON, RS-TROPOMI-KNMI-017, issue: 2.0, 2008.

17

18 Veefkind, J.P., Aben, I., McMullan, K., Förster, H., de Vries, J., Otter, G., Claas, J., Eskes, H.J.,
19 de Haan, J.F., Kleipool, Q., van Weele, M., Hasekamp, O., Hoogeveen, R., Landgraf, J., Snel, R.,
20 Tol, P., Ingmann, P., Voors, R., Kruizinga, B., Vink, R., Visser, H., and Levelt, P.F.: TROPOMI on
21 the ESA Sentinel-5 Precursor: A GMES mission for global observations of the atmospheric
22 composition for climate, air quality and ozone layer applications, *Remote Sensing of*
23 *Environment*, doi:10.1016/j.rse.2011.09.027, 2012.

24

25 Vountas, M., Rozanov, V. V. and Burrows, J. P.: Ring effect: impact of rotational Raman
26 scattering on radiative transfer in earth's atmosphere, *J. of Quant. Spec. and Rad. Trans.*,
27 60(6), 943-961, 36 1998.



1

2 Wang, Y., Beirle, S., Lampel, J., Koukouli, M., De Smedt, I., Theys, N., Xie, P. H., Van
3 Roozendael, M., and Wagner, T.: Validation of OMI and GOME-2A and GOME-2B
4 tropospheric NO₂, SO₂ and HCHO products using MAX-DOAS observations from 2011 to
5 2014 in Wuxi, China, submitted to Atmos. Chem. Phys. Discuss., 2016.

6

7 Wagner, T., Burrows, J. P., Deutschmann, T., Dix, B., von Friedeburg, C., Frieß, U., Hendrick,
8 F., Heue, K.-P., Irie, H., Iwabuchi, H., Kanaya, Y., Keller, J., McLinden, C. A., Oetjen, H., Palazzi,
9 E., Petritoli, A., Platt, U., Postlyakov, O., Pukite, J., Richter, A., van Roozendael, M., Rozanov,
10 A., Rozanov, V., Sinreich, R., Sanghavi, S., and Wittrock, F.: Comparison of box-air-mass-
11 factors and radiances for Multiple-Axis Differential Optical Absorption Spectroscopy (MAX-
12 DOAS) geometries calculated from different UV/visible radiative transfer models, Atmos.
13 Chem. Phys., 7, 1809-1833, 2007.

14

15 Wagner, T., Beirle, S., and Deutschmann, T.: Three-dimensional simulation of the Ring effect
16 in observations of scattered sun light using Monte Carlo radiative transfer models. *Atm.*
17 *Meas. Tech.*, 2, 113-124, 2009.

18

19 Yang, K., Krotkov, N., Krueger, A., Carn, S., Bhartia, P. K., and Levelt, P.: Retrieval of Large
20 Volcanic SO₂ columns from the Aura Ozone Monitoring Instrument (OMI): Comparisons and
21 Limitations, *J. Geophys. Res.*, 112, D24S43, doi:10.1029/2007JD008825, 2007.

22

23 Yang, K., Liu, X., Bhartia, P., Krotkov, N., Carn, S., Hughes, E., Krueger, A., Spurr, R., Trahan, S.:
24 Direct retrieval of sulfur dioxide amount and altitude from spaceborne hyperspectral UV
25 measurements: Theory and application, *J. Geophys. Res.*, 115, D00L09,
26 doi:10.1029/2010JD013982, 2010.

27



1 Yang, K., Dickerson, R. R., Carn, S. A., Ge, C., and Wang, J.: First observations of SO₂ from the
2 satellite Suomi NPP OMPS: Widespread air pollution events over China, Geophys. Res. Lett.,
3 40, 4957–4962, doi:10.1002/grl.50952.

4

5 Zhou, Y., Brunner, D., Boersma, K. F., Dirksen, R., and Wang, P.: An improved tropospheric
6 NO₂ retrieval for OMI observations in the vicinity of mountainous terrain, Atmos. Meas.
7 Tech., 2, 401-416, doi:10.5194/amt-2-401-2009, 2009.

8 Zweers, D. (editor) et al.: TRAQ Performance Analysis and Requirements Consolidation for
9 the Candidate Earth Explorer Mission TRAQ, Final report, KNMI, RP-ONTRAQ-KNMI-051,
10 issue: 1.0, 2010.

11 Zweers, S., et al., S5P ATBD for the UV aerosol index, available at:
12 <https://sentinel.esa.int/web/sentinel/technical-guides/sentinel-5p/appendices/references>
13 and <http://www.tropomi.eu/documents/level-2-products>, 2016.

14

15

16

17

18

19

20

21



1 Table 1. Requirements on SO₂ vertical column products as derived from the MRTD. Numbers
 2 denote accuracy / precision, respectively.

3

	Horizontal resolution [km]	Required uncertainty	Achievable uncertainty	Theme (Table in MRTD)
Enhanced stratospheric column	50-200	30% for VCD>0.5 DU	Met for VCD > 0.5DU	A3
Tropospheric column	5-20	30-60% or 1.3 x 10 ¹⁵ molecules cm ⁻² (least stringent)	50% / 3-6 x 10 ¹⁶ molec. cm ⁻²	B1, B2, B3
Total column	5-20	30-60% or 1.3 x 10 ¹⁵ molecules cm ⁻² (least stringent)	50% / 3-6 x 10 ¹⁶ molec. cm ⁻²	B1, B2, B3

4

5

6

7

8

9

10

11

12

13

14



1 Table 2. DOAS settings used to retrieved SO₂ slant columns

2

Fitting intervals 1 and 2	312-326 nm (w1), 325-335 nm (w2)
<i>Cross-sections</i>	SO ₂ : 203K (<i>Bogumil et al.</i> , 2003) O ₃ : 228K and 243K with <i>lo</i> correction (<i>Brion et al.</i> , 1998) Pseudo O ₃ cross sections ($\lambda\sigma_{O_3}$, $\sigma_{O_3^2}$) (<i>Puķīte et al.</i> , 2010) Ring effect: 2 eigenvectors (<i>Vountas et al.</i> , 1998) generated for 20° and 87° solar zenith angles using LIDORT-RRS (<i>Spurr et al.</i> , 2008)
<i>Polynomial</i>	5 th order
Fitting interval 3	360-390 nm (w3)
<i>Cross-sections</i>	SO ₂ : <i>Hermans et al.</i> (2009) extrapolated at 203K NO ₂ : 220K (<i>Vandaele et al.</i> , 1998) O ₂ -O ₂ : <i>Greenblatt et al.</i> , 1990 Ring effect: single spectrum (<i>Chance and Spurr</i> , 1997)
<i>Polynomial</i>	4 th order
Intensity offset correction	Linear offset
Spectrum shift and stretch	Fitted
Spectral spikes removal procedure	<i>Richter et al.</i> [2011]
Reference spectrum	Baseline: Daily solar irradiance Foreseen update: Daily averaged earthshine spectrum in Pacific region (10°S-10°N, 160°E-120°W); separate spectrum for each detector row. NRT: averaged spectra of the last available day, Off-line: averaged spectra of the current day



Table 3. Criteria for selecting alternative fitting windows.

Window number	w1	w2	w3
Wavelength range	312 – 326 nm	325-335 nm	360-390 nm
Derived slant column	S1	S2	S3
Application	Baseline for every pixel	S1 > 15 DU and S2 > S1	S2 > 250 DU and S3 > S2

- 1
- 2
- 3
- 4
- 5
- 6
- 7
- 8
- 9
- 10
- 11
- 12



Table 4. Physical parameters that define the WF look-up table.

Parameter	Number of grid points	Grid values	Symbol
Atmospheric pressure [hPa]	64	1056.77, 1044.17, 1031.72, 1019.41, 1007.26, 995.25, 983.38, 971.66, 960.07, 948.62, 937.31, 926.14, 915.09, 904.18, 887.87, 866.35, 845.39, 824.87, 804.88, 785.15, 765.68, 746.70, 728.18, 710.12, 692.31, 674.73, 657.60, 640.90, 624.63, 608.58, 592.75, 577.34, 562.32, 547.70, 522.83, 488.67, 456.36, 425.80, 396.93, 369.66, 343.94, 319.68, 296.84, 275.34, 245.99, 210.49, 179.89, 153.74, 131.40, 104.80, 76.59, 55.98, 40.98, 30.08, 18.73, 8.86, 4.31, 2.18, 1.14, 0.51, 0.14, 0.03, 0.01, 0.001	p_i
Altitude corresponding to the atmospheric pressure, using a US standard atmosphere [km]	64	-0.35, -0.25, -0.15, -0.05, 0.05, 0.15, 0.25, 0.35, 0.45, 0.55, 0.65, 0.75, 0.85, 0.95, 1.10, 1.30, 1.50, 1.70, 1.90, 2.10, 2.30, 2.50, 2.70, 2.90, 3.10, 3.30, 3.50, 3.70, 3.90, 4.10, 4.30, 4.50, 4.70, 4.90, 5.25, 5.75, 6.25, 6.75, 7.25, 7.75, 8.25, 8.75, 9.25, 9.75, 10.50, 11.50, 12.50, 13.50, 14.50, 16.00, 18.00, 20.00, 22.00, 24.00, 27.50, 32.50, 37.50, 42.50, 47.50, 55.00, 65.00, 75.00, 85.00, 95.00	z_i
Solar zenith angle [°]	17	0, 10, 20, 30, 40, 45, 50, 55, 60, 65, 70, 72, 74, 76, 78, 80, 85	θ_0
Line of sight angle [°]	10	0, 10, 20, 30, 40, 50, 60, 65, 70, 75	θ
Relative azimuth angle [°]	5	0, 45, 90, 135, 180	ϕ
Total ozone column [DU]	4	205, 295, 385, 505	TO3
Surface albedo	14	0, 0.01, 0.025, 0.05, 0.075, 0.1, 0.15, 0.2, 0.25, 0.3, 0.4, 0.6, 0.8, 1.0	A_s
Surface / cloud top pressure [hPa]	17	1063.10, 1037.90, 1013.30, 989.28, 965.83, 920.58, 876.98, 834.99, 795.01, 701.21, 616.60, 540.48, 411.05, 308.00, 226.99, 165.79, 121.11	p_s
AMF Wavelength	3	313, 326, 375	

1

2

3

4

5



Table 5. Systematic and random error components contributing to the total uncertainty on the SO₂ slant column.

#	Error source	Type*	Parameter uncertainty	Typical uncertainty on SO ₂ SCD
1	SO ₂ absorption cross section	S	6% (window 1) 6% (window 2) unknown (window 3)	6%
2	SO ₂ and O ₃ absorption	S & R		Errors 9 & 10
3	Other atmospheric absorption or interference	S & R		Error 9
4	Radiance shot noise	R	S/N=800-1000	0.3-0.5 DU (window 1) 5 DU (window 2) 60 DU (window 3)
5	DOAS settings	S	1 nm, polynomial order	<11% (window 1) <6% (window 2) <8% (window 3)
6	Wavelength and radiometric calibration	S	Wavelength Calibration. Radiometric calibration. Additive errors should remain below 2 %.	Wavelength calibration and spectral shifts can be corrected by the algorithm to less than 5 % effect on the slant column. Intensity offset correction in principle treats (small) radiometric calibration errors
7	Spectral response function		TBD	TROPOMI-specific Expected uncertainty: 10%
8	Other spectral features		Strongly dependent on interfering signal	-
9	Background correction	S & R		0.2 DU

* R: random, S: systematic



Table 6. Systematic and random error components contributing to the total uncertainty on the SO₂ air mass factor.

#	Error	Type*	Parameter uncertainty	Typical uncertainty on the AMF
10	AMF wavelength dependence	S		10%
11	Model atmosphere	S	O ₃ profile P,T profiles	~5-10% small
12	Forward model	S	< 5%	<5%
13	Surface albedo [†]	S	0.02	15% (PBL) 5% (FT) 1% (LS)
14	Cloud fraction [†]	R	0.05	5% (PBL) 15% (FT) 1% (LS)
15	Cloud top pressure [†]	R	50 hPa	50% (PBL) 50% (FT) 1% (LS)
16	Cloud correction	R		< 5% on yearly averaged data
17	Cloud model		TBD	
18	SO ₂ profile shape	S		anthropogenic SO ₂ 20%-35% volcanic SO ₂ large (low albedo), < 50% (high albedo)
19	Aerosol	S & R		Anthropogenic SO ₂ < 15% (Nowlan et al., 2011). Volcanic SO ₂ (aerosols: ash/sulphate) : ~ 20% (Yang et al., 2010)
20	Temperature correction	R		~5%

* R: random, S: systematic

[†] Effect on the AMF estimated from Figure 6



- 1 Table A1. List of output fields in the TROPOMI SO₂ products. nAlong x nAcross corresponds
- 2 to the number of pixels in an orbit along track and across track, respectively.

Name/Data	Symbol	Unit	Description	Data type	Number of entries per observation
Date		n.u.	Date and time of the measurement YYMMDDHHMMSS.MS	characters	nAlong
Latitudes	<i>lat</i>	degree	Latitudes of the four pixel corners + center	float	5 x nAlong x nAcross
Longitudes	<i>lon</i>	degree	Longitudes of the four pixel corners + center	float	5 x nAlong x nAcross
SZA	θ_0	degree	Solar zenith angle	float	nAlong x nAcross
VZA	θ	degree	Viewing zenith angle	float	nAlong x nAcross
RAA	φ	degree	Relative azimuth angle	float	nAlong x nAcross
SCD	N_s	mol.m ⁻²	SO ₂ slant column density	float	nAlong x nAcross
SCDcorr	N_s^c	mol.m ⁻²	SO ₂ slant column density background corrected	float	nAlong x nAcross
VCD	N_v	mol.m ⁻²	SO ₂ vertical column density (4values)	float	4 x nAlong x nAcross
Wdow flag	<i>Wflag</i>	n.u.	Flag for the fitting window used (1,2,3)	integer	nAlong x nAcross
AMF	<i>M</i>	n.u.	Air mass factor (4values)	float	4 x nAlong x nAcross
Cloud free AMF	M_{clear}	n.u.	Cloud Free Air mass factor (4values)	float	4 x nAlong x nAcross
Cloudy AMF	M_{cloud}	n.u.	Fully Cloudy Air mass factor (4values)	float	4 x nAlong x nAcross
CF	f_c	n.u.	Cloud fraction	float	nAlong x nAcross
CRF	Φ	n.u.	Cloud radiance fraction	float	nAlong x nAcross



CP	p_{cloud}	Pa	Cloud top pressure	float	nAlong x nAcross
CH	z_{cloud}	m	Cloud top height	float	nAlong x nAcross
CA	A_{cloud}	n.u.	Cloud top albedo	float	nAlong x nAcross
Albedo	A_s	n.u.	Surface albedo	float	nAlong x nAcross
Aerosol index	AAI	n.u.	Absorbing Aerosol Index	float	nAlong x nAcross
Ch-squared	Chi^2	n.u.	Chi-squared of the fit	float	nAlong x nAcross
VCD error	σ_{N_v}	mol.m ⁻²	Total error on the vertical column (individual measurement)	float	4x nAlong x nAcross
SCD random error	$\sigma_{N_s_{rand}}$	mol.m ⁻²	Random error on the slant column	float	nAlong x nAcross
SCD systematic error	$\sigma_{N_s_{syst}}$	mol.m ⁻²	Systematic error on the slant column	float	nAlong x nAcross
AMF random error	$\sigma_{M_{rand}}$	n.u.	Random error on the air mass factor (4values)	float	4x nAlong x nAcross
AMF systematic error	$\sigma_{M_{syst}}$	n.u.	Systematic error on the air mass factor (4 values)	float	4x nAlong x nAcross
Averaging kernel	AK	n.u.	Total column averaging kernel (for a- priori profile from CTM)	float	34 x nAlong x nAcross
Averaging kernel scalings for box profiles	Scaling box	n.u.	Factors to apply to the averaging kernel function to obtain the corresponding averaging kernels for the 3 box profiles	float	3x nAlong x nAcross
SO₂ profile	n_a	n.u.	A-priori profile from CTM (volume mixing ratio)	float	34 x nAlong x nAcross
Surface altitude	z_s	m	Digital elevation map	float	nAlong x nAcross
Surface pressure	p_s	Pa	Effective surface pressure of the satellite pixel	float	nAlong x nAcross
TMS level coefficient a	A_i	Pa	TMS pressure level coefficients that effectively define the mid-layer levels	float	24



TM5 level coefficient b	A_i	n.u.	(from ECMWF)	float	24
------------------------------------	-------	------	--------------	-------	----

1

2

3

4

5

6

7

8

9

10

11

12

13

14

15



1 Table A2. Static auxiliary data for the S5P SO₂ algorithm.

Name/Data	Sym bol	Unit	Source	Pre-process needs	Comments
Absorption cross-sections					
SO₂	σ_{SO_2}	cm ² molec. ⁻¹	Bogumil et al. (2003), 203K, 223K, 243K, 293K Hermans et al. (2009), all temperatures	Convolution at the instrumental spectral resolution using the provided slit function	-
Ozone	$\sigma_{O_3 218}$ $\sigma_{O_3 243}$	cm ² molec. ⁻¹	Brion et al. (1998) ; 218K and 243K.		
BrO	σ_{BrO}	cm ² molec. ⁻¹	Fleischmann et al. (2004), 223K		
NO₂	σ_{NO_2}	cm ² molec. ⁻¹	Vandaele et al. (1998), 220K		
O₄ (O₂-O₂)	σ_{O_4}	cm ⁵ molec. ⁻²	Greenblatt et al. (1990)		
High resolution reference solar spectrum	E_s	W m ⁻² nm ⁻¹	Chance and Kurucz, 2010	-	-
Ring effect	$\sigma_{ringev1}$ $\sigma_{ringev2}$	cm ² molec. ⁻¹	2 Ring cross-sections generated internally.	A high-resolution reference solar spectrum and the instrument slit function are needed to generate the data set.	Calculated in an ozone containing atmosphere for low and high SZA, using LIDORT_RRS (Spurr et al., 2008) and a standard atmosphere (Camelot European Pollution atmospheric profile).
Non-linear O₃ absorption effect	$\sigma_{O_3 l}$ $\sigma_{O_3 sq}$	nm.cm ² molec. ⁻¹ cm ⁴ molec. ⁻²	2 pseudo-cross sections generated internally.	The O ₃ cross- section at 218 K is needed.	Calculated from the Taylor expansion of the wavelength and the O ₃ optical depth (Puķīte et al., 2010).
Instrument slit function	SF	n.u.	Slit Function by wavelength/detector.	-	Values between 300 and 400nm.
Surface Albedo	A_s	n.u.	OMI-based monthly minimum LER (update of Kleipool et al., 2008)	-	
Digital elevation map	z_s	m	GMTED2010 (Danielson et al., 2011)		Average over the ground pixel area.
SO₂ profile	n_a	n.u.	One kilometre thick box profiles, with three different peak altitudes,	-	TM5 profiles from the last available day in case the TM5 profiles of the



			<p>representing different altitude regimes:</p> <p>Boundary layer: from the surface altitude to 1km above it.</p> <p>Free troposphere: centred around 7 km altitude.</p> <p>Lower stratosphere: centred around 15 km altitude.</p> <p>Daily SO₂ profiles forecast from TM5</p>		current day are not available
Look-up table of pressure-resolved AMFs	<i>m</i>	n.u.	Calculated internally with the LIDORTv3.3 RTM (Spurr, 2008).	-	For the different fitting windows (312-326 nm, 325-335 nm, 360-390 nm), the assumed vertical column is 5 DU, 100 DU, 500 DU, respectively.
Temperature correction parameters	α	K ⁻¹	Bogumil et al. (2003)	-	-

1

2

3

4

5

6

7

8

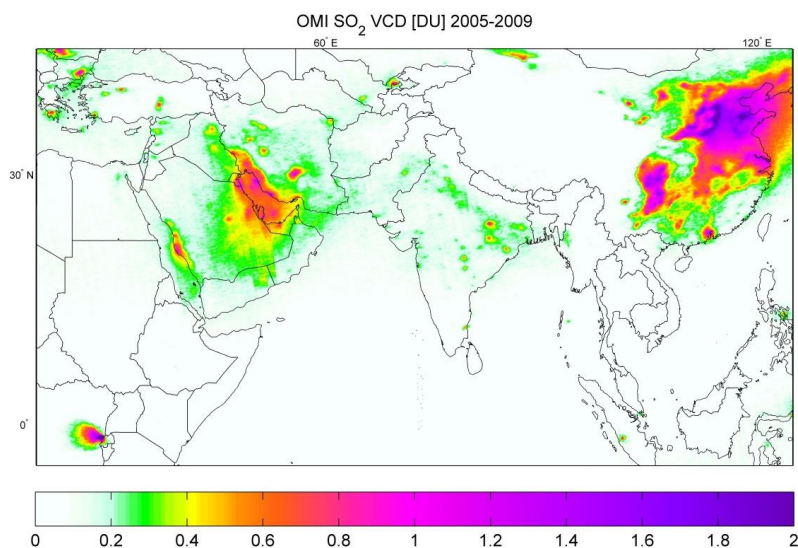
9



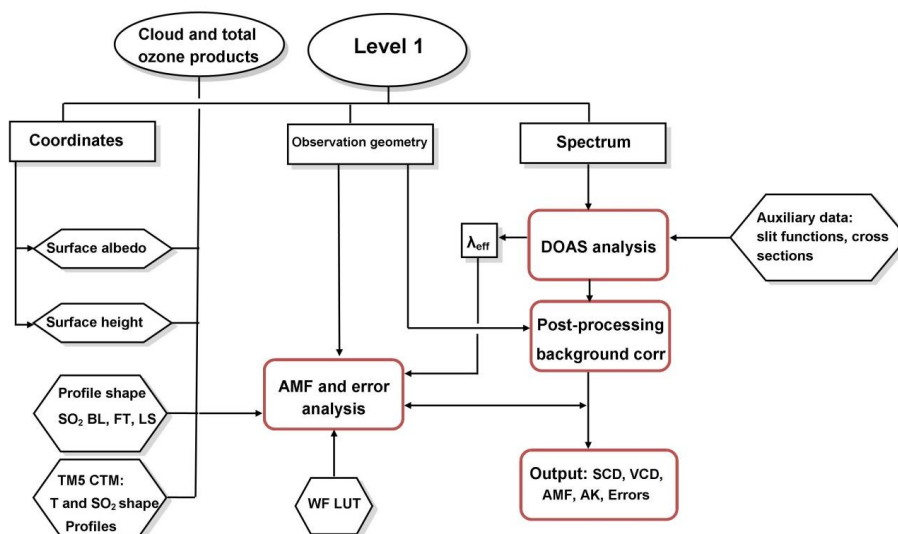
1 Table A3. Dynamic auxiliary data for the S5P SO₂ algorithm.

Name/Data	Symbol	Unit	Source	Pre-process needs	Backup if not available
S5P level 1B Earth radiance	I	$\text{mol s}^{-1} \text{m}^{-2} \text{nm}^{-1} \text{sr}^{-1}$	S5P L1b product	-	No retrieval
S5P level 1B sun irradiance	E_0	$\text{mol s}^{-1} \text{m}^{-2} \text{nm}^{-1}$	S5P L1b product	Wavelength recalibrated using a high-resolution reference solar spectrum	Use previous measurement
S5P Cloud fraction	f_c	n.u.	S5 P operational cloud product based on a Lambertian cloud model (Loyola et al., 2016) UPAS processor.	-	No retrieval
S5P Cloud top pressure	p_{cloud}	Pa			
S5P Cloud top albedo	A_{cloud}	n.u.			
SO ₂ profile	n_a	n.u.	Daily forecast from TM5 CTM run at KNMI.	-	Use TM5 CTM profile from last available day
Temperature profile	T	K	Daily forecast from TM5 CTM run at KNMI.	-	Use TM5 CTM profile from last available day
S5P Absorbing aerosol index	AAI	n.u.	S5P operational AAI product (Zweers et al., 2016). Used for flagging. KNMI processor.	-	Missing information flag.
Snow-ice flag		n.u.	Near real-time global Ice and Snow Extent (NISE) data from NASA.	-	Use snow/ice climatology.

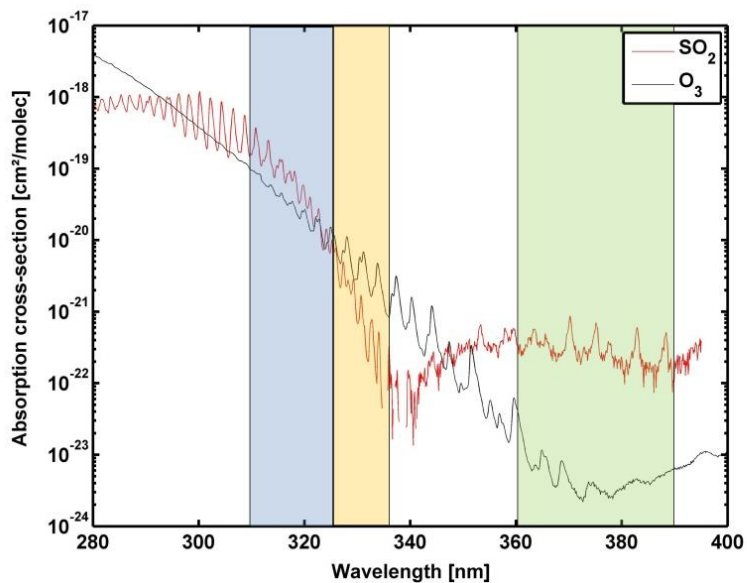
2



1
 2 Figure 1: Map of averaged SO₂ columns from OMI clear-sky pixels for the 2005-2009 period.

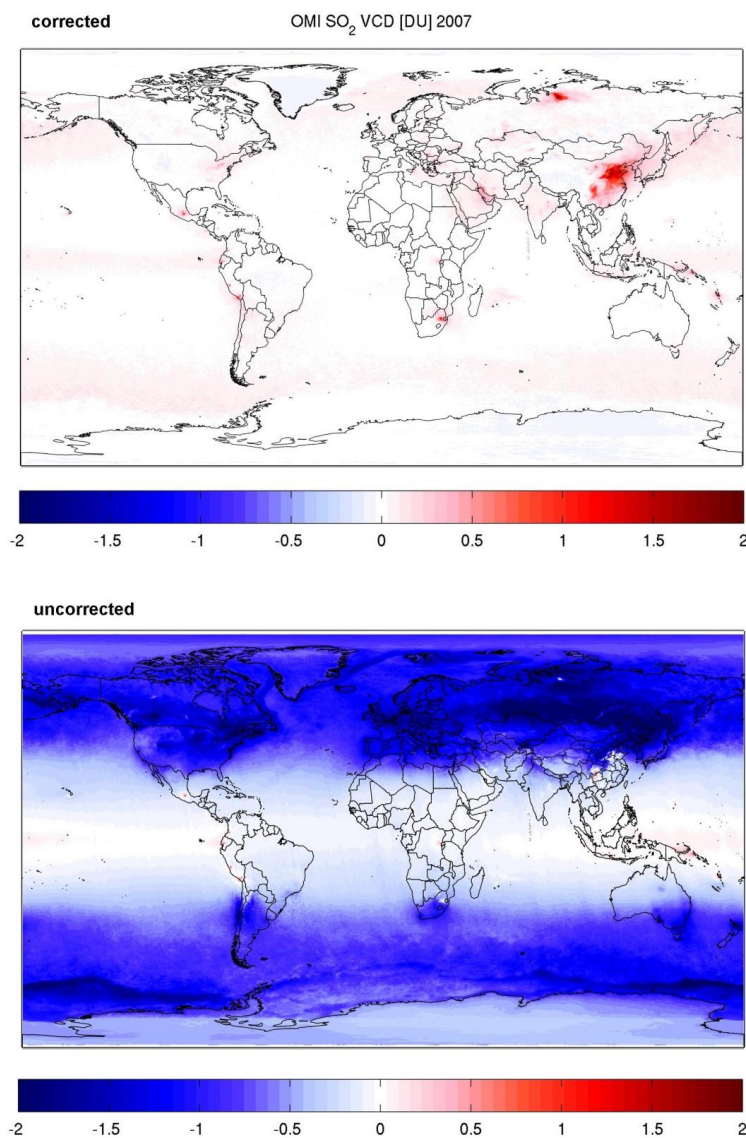


3
 4 Figure 2. Flow Diagram of the TROPOMI DOAS retrieval algorithm for SO₂.
 5



1

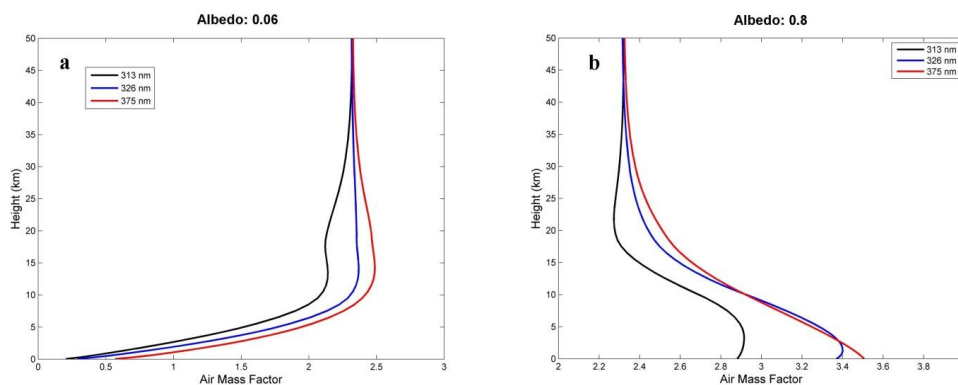
2 Figure 3. Absorption cross-sections of SO₂ and O₃. The blue, yellow and green boxes delimit
3 the three SO₂ fitting windows 312-326 nm, 325-335 nm and 360-390 nm, respectively.



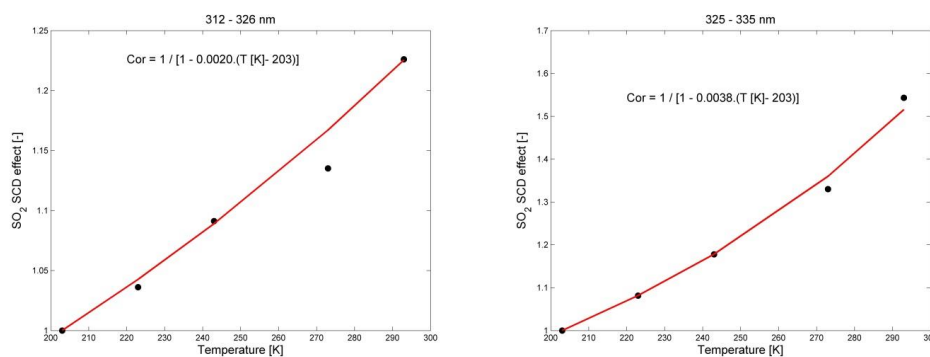
1

2

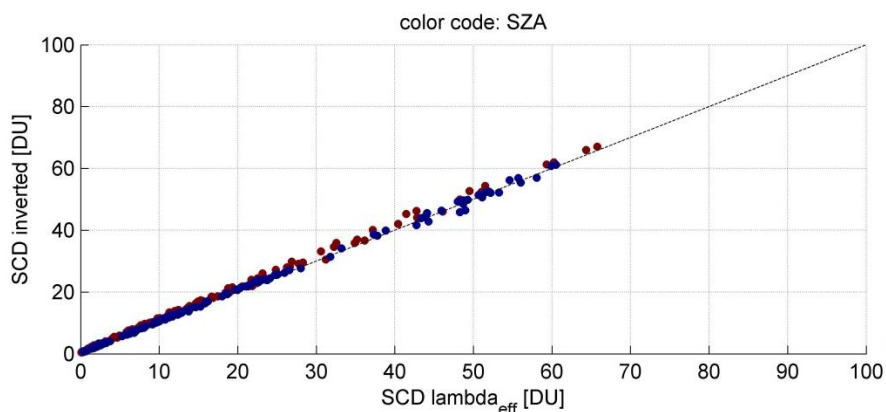
3 Figure 4. OMI SO₂ vertical columns (DU) averaged for the year 2007 (top) with and (bottom)
4 without background correction. Only clear sky pixels (cloud fraction lower than 30%) have
5 been kept. AMFs calculated from SO₂ profiles from the IMAGES global model are applied to
6 the slant columns (Theys et al., 2015).



- 1
- 2 Figure 5. SO₂ box-AMFs at 313, 326 and 375nm for albedo of (a) 0.06 and (b) 0.8. SZA: 40°,
- 3 LOS: 10°, RAA: 0°, Surface height: 0 km.



- 4 Figure 6. Effect of temperature (relative to 203K) on SO₂ retrieved SCD for fitting windows
- 5 312-326 nm (left) and 325-335 nm (right). The red lines show the adopted formulation of
- 6 C_{temp} (Eq. 10). Note that, for the 312-326 nm window, the result at 273K has been discarded
- 7 from the fit as it seems rather inconsistent with the dependence at other temperatures.
- 8



1

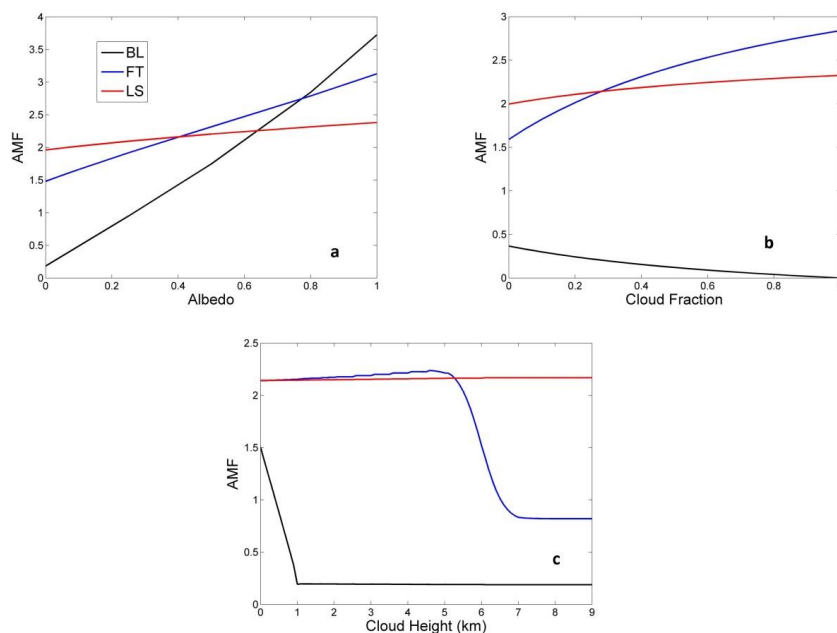
2 Figure 7. Retrieved SO_2 slant columns versus simulated SCDs at a wavelength of 313 nm from
3 synthetic spectra (SZA: 30° , 70°) in the spectral range 312-326 nm and for SO_2 layers in the
4 boundary layer, upper troposphere and lower stratosphere. The different points correspond
5 to different values for the line-of-sight angle (0° , 45°), surface albedo (0.06, 0.8), surface
6 height (0, 5 km) and total ozone column (350, 500 DU). SO_2 vertical columns as input of the
7 RT simulations are maximum of 25 DU.

8

9

10

11

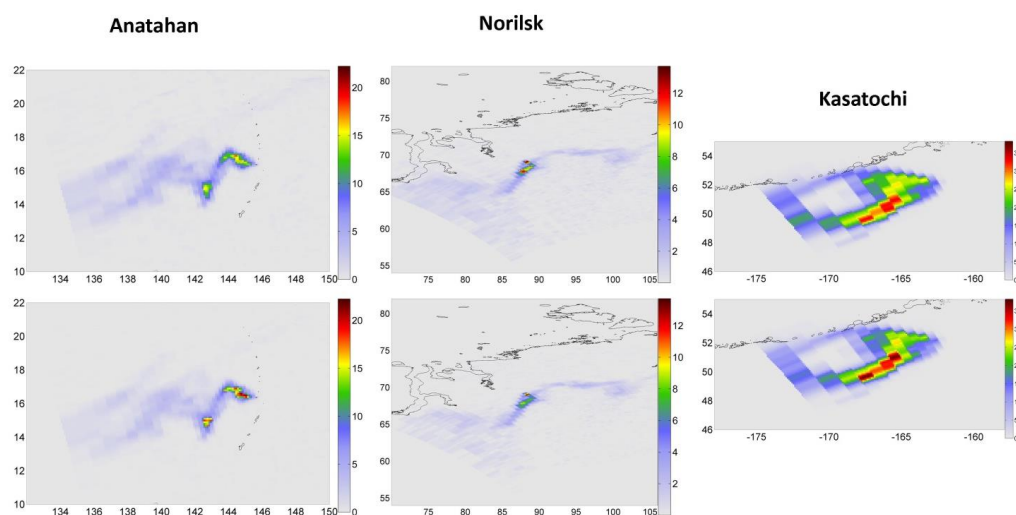


1

2 Figure 8. Air mass factors at 313 nm for SO₂ in the boundary layer (BL :0-1 km), free-
3 troposphere and lower stratosphere (FT, LS: Gaussian profiles with maximum height at 6,15
4 km and FWHM: 1 km). Calculations are for SZA=40°, Los=10°, RAA=0° and surface height=0
5 km. AMFs are displayed as a function of the (a) albedo for clear-sky conditions, (b) cloud
6 fraction for albedo=0.06, cloud albedo=0.8 and cloud top height=2km and (c) cloud top
7 height for albedo=0.06, cloud albedo=0.8 and cloud fraction=0.3.

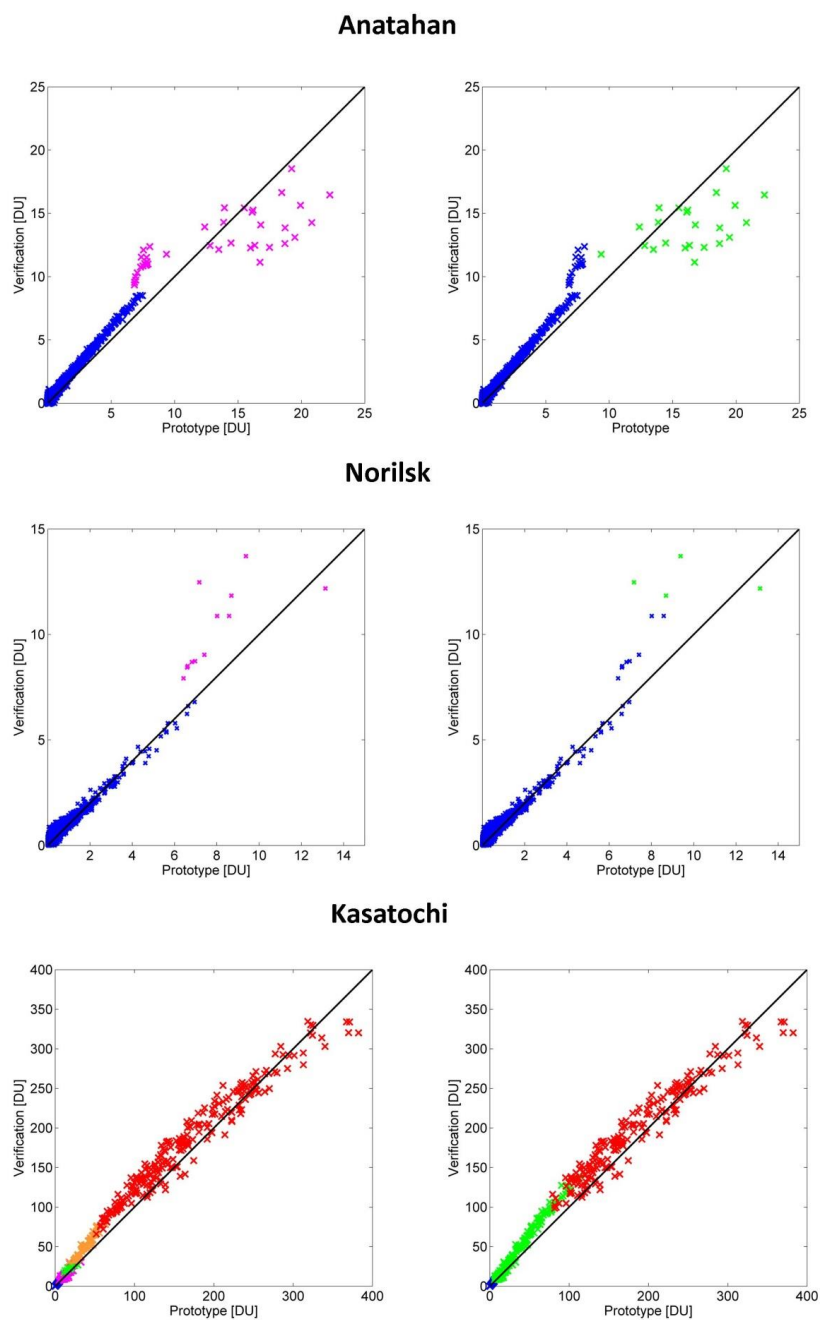
8

9



1

2 Figure 9. OMI SO₂ VCD (expressed in DU) for the Verification (upper panels) and Prototype
3 Algorithms (lower panels) for the three selected scenarios: during the Anatahan eruption
4 (left), over the Norilsk copper smelter area (center) and for the volcanic eruption of
5 Kasatochi (right). Note that, for each case, the colorbar has been scaled to the maximum SO₂
6 VCD from both algorithms.



1

2 Figure 10. OMI SO₂ VCD (DU) scatter plots for PA (x-axis) and VA (y-axis) for the three test
3 cases, Anatahan eruption, Norilsk anthropogenic emissions and Kasatochi eruption (from top



1 to bottom). The different fit windows used for both algorithms are color-coded: VA on left
2 panels (blue: SR, purple: SR/MR, green: MR, orange: MR/AR, red: AR), PA on right panels
3 (blue: 312-326 nm, green: 325-335 nm, red: 360-390 nm). For the three scenarios, the
4 prototype and verification algorithms agree fairly well with $r^2 \sim 0.9$.

5

6

7

8

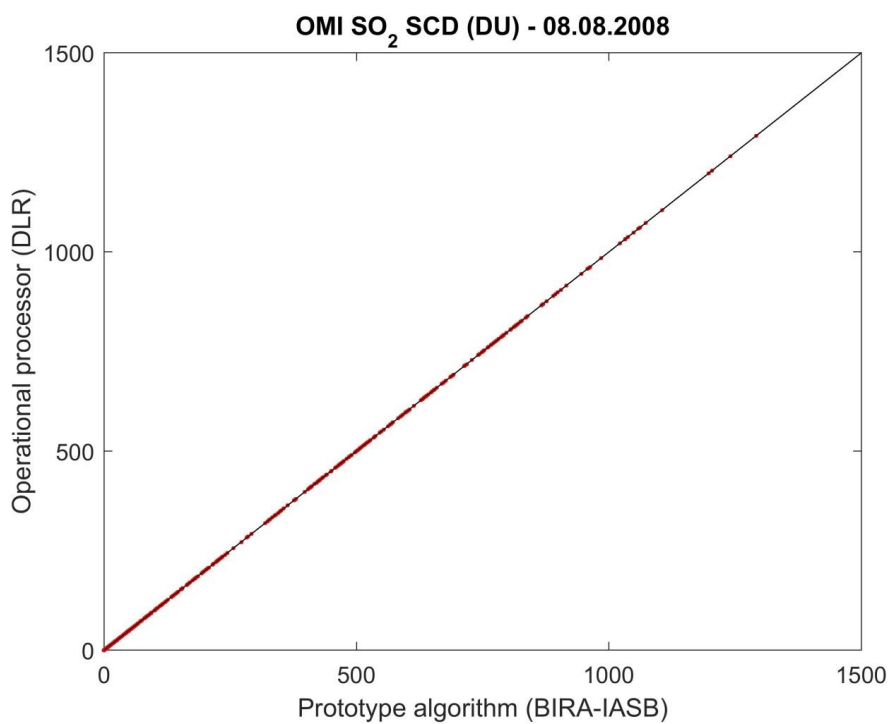
9

10

11

12

13



1

2 Figure 11. Comparison of SO₂ SCDs between prototype algorithm and operational processor
3 for the OMI test data of August 8, 2008.